

1-1-2008

Photo-Electrical Properties Of Semiconducting Se-Sb-In Thin Films

Maninder Kamboj
Ryerson University

Follow this and additional works at: <http://digitalcommons.ryerson.ca/dissertations>

 Part of the [Electrical and Computer Engineering Commons](#)

Recommended Citation

Kamboj, Maninder, "Photo-Electrical Properties Of Semiconducting Se-Sb-In Thin Films" (2008). *Theses and dissertations*. Paper 1139.

This Thesis is brought to you for free and open access by Digital Commons @ Ryerson. It has been accepted for inclusion in Theses and dissertations by an authorized administrator of Digital Commons @ Ryerson. For more information, please contact bcameron@ryerson.ca.

B19306295

TK
7871.15
FS
K36
2009

**PHOTO-ELECTRICAL PROPERTIES OF
SEMICONDUCTING Se-Sb-In THIN FILMS**

by

Maninder Kamboj

A Project

presented to Ryerson University
in partial fulfillment of the
requirement for the degrees of
Master of Engineering
in the program of
Electrical and Computer Engineering

Toronto, Ontario, Canada 2008

© Maninder Kamboj 2008

PROPERTY OF
RYERSON UNIVERSITY LIBRARY

Author's Declaration

I hereby declare that I am the sole author of this project.

I authorize Ryerson University to lend this project to other institutions or individuals for the purpose of scholarly research.

Signature

I further authorize Ryerson University to reproduce this project by photocopying or by other means, in total or in part, at the request of other institutions or individuals for the purpose of scholarly research.

Signature

Instructions on Borrowers

Ryerson University requires the signature of all persons using or photocopying this project.

Please sign below, and give address and date.

Abstract

The objective of this research project was to analyze the photo-degradation of the photocurrent of the electron beam evaporated amorphous semiconducting $\text{Se}_{90-x}\text{Sb}_{10}\text{In}_x$ ($0 \leq x \leq 15$) thin films ($\alpha\text{-Se}_{90-x}\text{Sb}_{10}\text{In}_x$). The photo-induced effects in amorphous semiconducting $\text{Se}_{90-x}\text{Sb}_{10}\text{In}_x$ ($0 \leq x \leq 15$) thin films were studied using two approaches: *steady state* and *transient* photoconductivity. The degradation of photocurrent has been explained on the basis of theoretical models.

The steady state analysis has been performed by plotting the photocurrent (I_{ph}) versus light intensity (F) and this variation follows a power law $I_{\text{ph}} = F^\gamma$. The value of exponent γ lies between 0.5 and 1.0, which indicates there exists a continuous distribution of localized states in the mobility gap of $\text{Se}_{90-x}\text{Sb}_{10}\text{In}_x$ ($0 \leq x \leq 15$) thin films.

For transient photoconductivity, when the samples were illuminated with light, the photocurrent quickly reaches the maximum value and thereafter, it starts decreasing with the exposure period and becomes stable after approximately 15 minutes of exposure. This kind of phenomenon is termed as photodegradation of photocurrent. The results have been explained on the basis of charged defect model and the inter-cluster interaction model. High photocurrents are found for $\alpha\text{-Se}_{75}\text{Sb}_{10}\text{In}_{15}$ system, which is even higher than the parent system $\text{Se}_{90}\text{Sb}_{10}$.

The influence of bias voltage on the dark current and photocurrent of the $\text{Se}_{90-x}\text{Sb}_{10}\text{In}_x$ ($0 \leq x \leq 15$) thin films is also investigated. Both the dark and photocurrent increase with increase in the bias voltage.

The compositional dependence of dark conductivity, photoconductivity and the photosensitivity shows a minimum at 5 atomic percentage of Indium (In) concentration, which has been explained based on chemically ordered network model and the topological model.

Acknowledgements

I would like to thank my revered supervisor Prof. Farah Mohammadi for giving me an opportunity to do an M.Eng project under her able guidance. Without her tremendous motivation and constant encouragement, it would have been challenging to conduct this project work.

I would also like to thank to faculty and staff of Department of Electrical and Computer Engineering and the library staff for helping me in one or the other way during the tenure of this project.

I would like to thank my examination committee member Dr. Xavier Fernando for his great advices provided to me.

I am also thankful to Department of Applied Physics, Guru Nanak Dev University, India, where the experimental part of this work was carried out.

The help and encouragement provided by my friends, Niaz Khawaza, Mahboob, Adeel Afzal and Hartej Sidhu is kindly acknowledged.

I appreciate the patience of my family especially my daughter Japneer and my son Tejnoor during the time I was involved in carrying out this project. The morale support given by my wife Kawalpreet is also greatly regarded.

Above all, words cannot express my sincere thanks to the almighty God for showering countless blessings to me.

Table of Contents

Abstract.....	iv
Acknowledgements.....	v
List of Figures.....	viii
List of Tables.....	ix
10.....	9
Chapter 1.....	1
1 Introduction and Motivation.....	1
1.1 An overview of amorphous materials.....	1
1.2 Disorder and its types.....	2
1.3 Glass.....	2
1.4 Classification and applications of amorphous semiconductors (a- semiconductors).....	6
1.5 Basic physical process.....	12
1.6 Background on chalcogenide semiconductors.....	13
1.7 Thesis objectives.....	14
1.8 Thesis outline.....	16
Chapter 2.....	17
2 Theoretical Background.....	17
2.1 Electronic structure and charged defect state models.....	17
2.2 Cohen – Fritzsche - Ovshinsky (CFO) Model.....	18
2.3 Davis and Mott’s Model.....	20
2.4 Defect states in the band gap of chalcogenide elements and Compounds.....	21
2.5 Doping of amorphous chalcogenide glassy semiconductors.....	26
2.5.1 The addition of foreign additive after equilibration.....	27
2.5.2 Non-equilibrium modification of chalcogenides.....	28
2.6 General conduction mechanism (temperature dependence of DC conductivity) 29	
2.7 Absorption edge of amorphous chalcogenide semiconductors.....	32
2.7.1 High absorption region.....	33
2.7.2 Exponential region of the absorption edge.....	35
2.7.3 Weak absorption tail.....	36
Chapter 3.....	37
3 Explanation of Experimental Set-up Used to Obtain the Analysed Data.....	37
3.1 Preparation of bulk samples.....	37
3.1.1 Weight calculations for 3 grams of Se ₉₀ Sb ₁₀ composition.....	38
3.1.2 Weight calculations for 3 grams of Se ₈₅ Sb ₁₀ In ₅ composition.....	38
3.1.3 Weight calculations for 3 grams of Se ₈₀ Sb ₁₀ In ₁₀ composition.....	39
3.1.4 Weight calculations for 3 grams of Se ₇₅ Sb ₁₀ In ₁₅ composition.....	40
3.2 Preparation of thin films.....	41
3.2.1 Thickness measurements of thin films.....	41
3.3 X-ray diffraction (XRD).....	44
3.4 Rutherford backscattering (RBS).....	44
3.5 DC conductivity and photoconductivity.....	45

3.5.1	DC conductivity set-up	45
3.5.2	Photoconductivity	47
3.6	Optical spectra	47
Chapter 4	49
4	Results and Discussion	49
4.1	Structure of bulk and thin films of $\text{Se}_{90-x}\text{Sb}_{10}\text{In}_x$ ($0 < x < 15$) system	49
4.2	Composition analysis by 'Rutherford back scattering technique	52
4.3	Photo-electrical properties of amorphous Se-Sb-In thin films	52
4.4	Steady state photoconductivity	54
4.5	Transient photoconductivity	56
4.6	Compositional dependence of photocurrent of $\text{Se}_{90-x}\text{Sb}_{10}\text{In}_x$ ($0 < x < 15$) thin films	56
4.7	Charged defect model	60
4.8	Inter-cluster interaction model	62
4.9	Influence of bias voltage on dark current and photocurrent of $\text{Se}_{90-x}\text{Sb}_{10}\text{In}_x$ ($0 < x < 15$) thin films	64
4.10	Compositional dependence of dark conductivity, photoconductivity and photosensitivity	66
Chapter 5	71
5	Summary and Conclusions	71
5.1	Scope of future work	72
6	References	74
7	List of publications	80

List of Figures

Figure 1.1 Classification of disorder.....	3
Figure 1.2 Schematic representation of various types of disorders: (a) Substitutional disorder (b) Structural disorder (c) Topological disorder [Ref. 4].....	4
Figure 1.3 Schematic illustration of the free energy versus configuration [Ref. 49].....	7
Figure 1.4 Volume versus temperature curve for glass forming systems: T_g : glass transition temperature, T_m : melting temperature [Ref 4].....	8
Figure 1.5 Schematic representations of transformations between states with crystalline, intermediate and amorphous atomic structures. The energy barriers between the states can be traversed in either direction by the application of energy pulse profiles [Ref. 8].....	11
Figure 2.1 Sketch of the electronic density of states of (a) a perfect crystalline chalcogen solid (b) an ideal amorphous chalcogen solid [Ref. 4]	19
Figure 2.2 The density of states diagrams for amorphous semiconductors in different models: (a) CFO model (b) Davis-Mott model (c) Modified Davis-Mott model (d) A real glass with defect states [Ref. 49].	22
Figure 2.3 (a) and (b) Illustration of the transfer of an electron from one chain end to another creating two charged defects D^+ and D^- (c) The positive correlation energy U associated with two electron, electrons at one site turned into an effective negative correlation energy U associated with two electron, electrons at one site turned into an effective negative correlation energy U_{eff} because of the configurational changes, “q” is configurational coordinate [Ref. 49].....	23
Figure 2.4 Temperature dependence of dc conductivity in a-semiconductor on the basis of Davis-Mott model. The regions marked as A, B, C and D corresponds to conduction occurring dominantly at the energies shown on the right [Ref. 49].....	30
Figure 2.5 (a) Absorption edge in amorphous semiconductors (b) Density of states $N(E)$ as a function of energy E in amorphous semiconductors [Ref. 61].	34
Figure 3.1 (a) Thickness measurement setup (b) Pattern of fringes with the step.....	43
Figure 3.2 Schematic diagram of the dc conductivity and photoconductivity set-up.....	46
Figure 4.1 XRD pattern of bulk $Se_{90-x}Sb_{10}In_x$ ($0 \leq x \leq 15$).....	50
Figure 4.2 XRD pattern of $Se_{90-x}Sb_{10}In_x$ ($0 \leq x \leq 15$) thin films	51
Figure 4.3 Variation of photo current I_{ph} with light intensity F for.....	55
Figure 4.4 Transient photoconductivity of $Se_{90}Sb_{10}$	57
Figure 4.5 Transient photoconductivity of $Se_{90-x}Sb_{10}In_x$ ($x = 15$).....	58
Figure 4.6 Compositional dependence of photocurrent versus exposure time	59
Figure 4.7 Compositional dependence of photocurrent versus exposure time	59
Figure 4.8 Configuration coordinate diagram.....	61
Figure 4.9 Schematic diagram of inter-cluster interaction model (a) Normal bonding (b) Structure influenced by light illumination	63
Figure 4.10 Variation of bias voltage with current of $Se_{90}Sb_{10}$	65
Figure 4.11 Variation of bias voltage with current of $Se_{75}Sb_{10}In_{15}$	65
Figure 4.12 Variation of dark conductivity (σ_d) and photoconductivity (σ_{ph}) with composition.....	68

Figure 4.13 Composition/Average coordination dependence of photosensitivity of $\text{Se}_{90-x}\text{Sb}_{10}\text{In}_x$ ($0 \leq x \leq 15$) thin films	70
--	----

List of Tables

Table 1.1 Classification of amorphous semiconductors [Ref. 4].....	10
Table 2.1 Structure and energy of various defect configurations in a two-fold coordinated material. Arrow represents the spin of electron. In column two, C refers to the chalcogenide atom, the superscript is the charged state and subscript is number of neighbouring atoms [Ref. 44]	24
Table 3.1 Thickness of $\text{Se}_{90-x}\text{Sb}_{10}\text{In}_x$ ($0 \leq x \leq 15$) thin films measured by Tolansky's method.....	42
Table 4.1 Results of RBS and error percentage in composition.....	53
Table 4.2 Differential conductance of $\text{Se}_{90-x}\text{Sb}_{10}\text{In}_x$ ($0 \leq x \leq 15$) thin films at room temperature at 1000 lx	67

Chapter 1

1 Introduction and Motivation

An introduction to amorphous semiconductors, their classifications and technological applications are briefly summed up in this chapter. The objectives of present investigations are also included in this chapter.

1.1 An overview of amorphous materials

Amorphous materials are not new from structure point of view. The introduction of iron-rich siliceous glassy materials recovered from the moon by one of the Apollo missions are few billions years old [1] and man has been manufacturing glassy materials for about thousands of years.

Materials in general can be classified as amorphous or crystalline. The structure of amorphous solid is characterized as an irregular arrangement of atoms in contrast with crystalline solids whose structure has a periodic array of atoms [2]. When the periodicity of the atoms extends throughout a certain portion of material, one can speak of a single crystal. In polycrystalline materials, the periodicity of the structure is interrupted at the so-called grain boundaries. When the size of grain boundary or a crystallite becomes comparable to the size of the pattern unit, one can no longer speak of crystals, since the essential feature of the crystal is the periodicity of the structure; one then speaks of non-

crystalline materials. As a matter of fact, any material, which does not meet the above criterion of a periodicity of atoms, is non-crystalline.

1.2 Disorder and its types

Disorder is classified as compositional disorder, structural disorder and topological disorder. The compositional disorder occurs when the constituent atoms in crystalline binary alloy are randomly substituted into lattice sites, so this is also called substitutional disorder. Substitutional disorder is found in substitutional alloys and mixed crystals. Structural disorder is found in liquid and amorphous metals and topological disorder is found in amorphous semiconductors. Such substances lack translational periodicity and the position of the atoms is not regular in these systems. The connectivity of the covalent bonds (which defines a random network) plays an important role in determining some physical properties of these systems, as in amorphous solid semiconductors. The positions of the atoms are disordered, and long-range order is absent. However, the short-range order is preserved in a way similar to their crystalline counterparts. The bond-lengths and bond-angles fluctuate around respective average value corresponding to those found in ordered crystals. The particle positions are totally uncorrelated and the system has complete disorder in case of dilute gasses. The classification of disorder is given in Fig. 1.1. The diagrammatic representation of various types of disorders is given in Fig. 1.2 (a, b and c).

1.3 Glass

Different types of glasses are under discussion these days. The general concept of glass relates to systems, which have some degree of freedom that (1) fluctuate at a rate, which depends on temperature or pressure and that (2) becomes so slow at low temperature or high pressure that the fluctuations becomes frozen. At this point, properties determined by the slow degree of freedom change value more or less abruptly, gives the glass transition. In spin glasses, it is the magnetic susceptibility, which decreases suddenly as the fluctuations in magnetization freezes in, while with glass forming liquids, it is the heat capacity, compressibility and dielectric susceptibility. Thus most general definition -

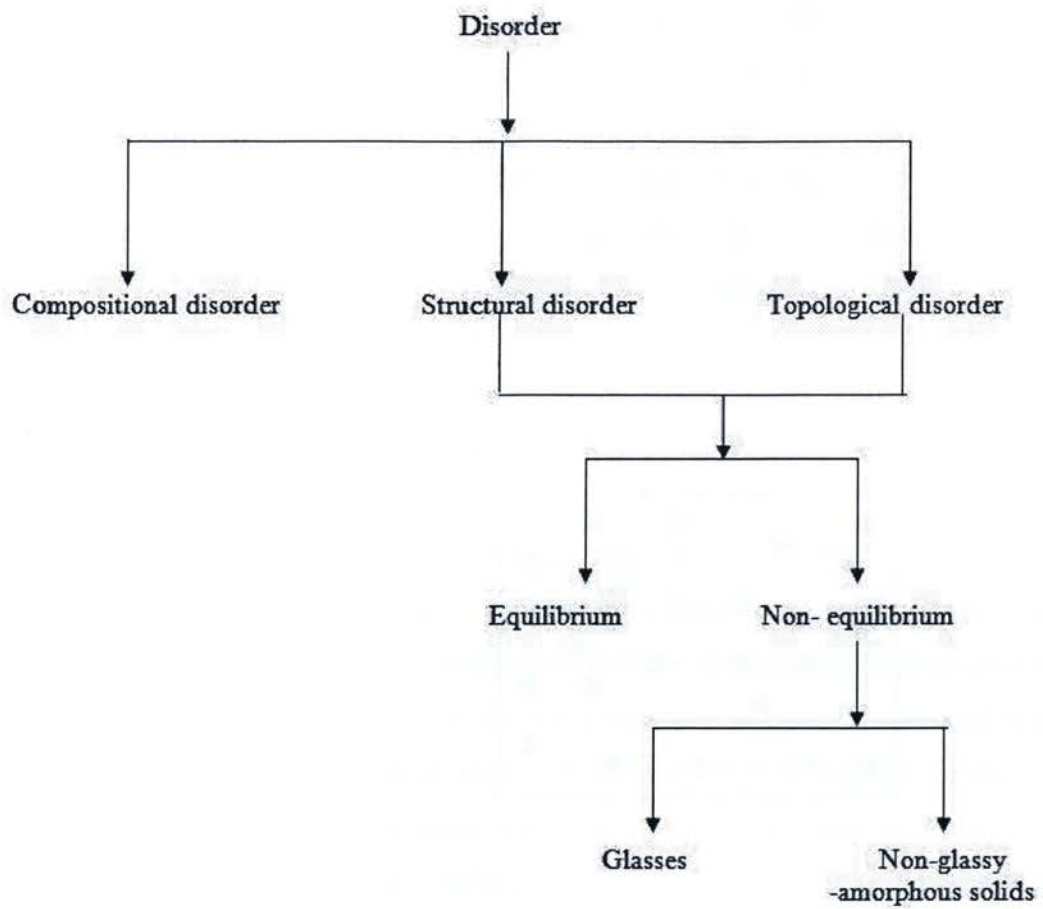
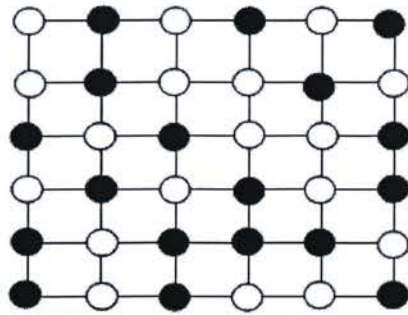
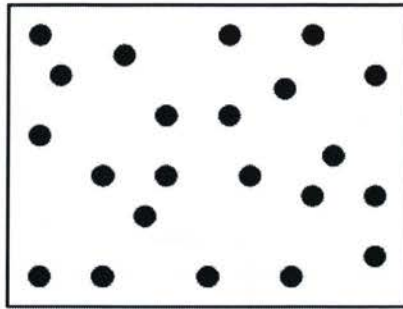


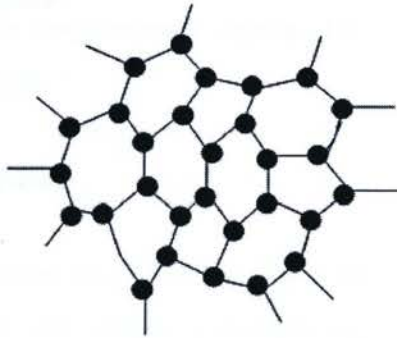
Figure 1.1 Classification of disorder



(a) Substitutional Disorder



(b) Structural Disorder



(c) Topological Disorder

Figure 1.2 Schematic representation of various types of disorders: (a) Substitutional disorder (b) Structural disorder (c) Topological disorder [Ref. 4]

- of glass is "A glass is a condensed matter which has become non-ergodic by virtue of the continuous slow down of one or more degrees of freedom. Satisfying this definition there are spin glasses and orientation glasses (dipole, quadrupole and octapole) and vortex glasses, which themselves are now known as structural glasses.

According to Elliott [1], the definition of glass is as follows "the term amorphous or equivalently no-crystalline, applies generally to those materials lacking the long-range translational periodicity characteristics of crystals, whereas the term glassy, or vitreous is reserved only for those materials which exhibit a glass transition temperature ' T_g '. Exemplified by some synthetic polymers, ordinary window glass, optical fibers and gels, glassy materials are considered to be among the least understood systems in solid-state physics.

The crystalline materials show sharp peaks in their X-ray diffraction (XRD) pattern. Whereas in case of amorphous materials only few broad humps (diffused pattern) are observed in XRD pattern. The coordination number of each atom in amorphous solid is the same as found in a crystal except for occasional deviation associated with the specific defects. The essential point about amorphous solids is that they exist in non-equilibrium states. This is the only main reason why amorphous semiconductors are very interesting. The energy versus configuration variation indicating amorphous and crystalline state is shown in fig. 1.3. Point C gives the minimum energy level corresponding to a crystalline state. On the other hand, A_1 , A_2 , A_3 and A_4 are quasi minima or local minima corresponding to different metastable states. Various points of local minima correspond to different metastable states, which are brought out by different conditions during the formation process. These minimum states are separated from the state C with some barriers. External perturbations such as thermal, optical, electrical and mechanical agitations etc. cause the metastable states (A_1 , A_2 , A_3 and A_4) to equilibrium state (state C).

Amorphous materials can be prepared by different methods, e.g., quenching from the melt, thermal evaporation, sputtering etc. Based on their preparation methods, amorphous materials can be classified as glasses and non-glasses. When the temperature decreases from their liquid phase, some materials do not crystallize below their melting temperature, but they become super-cooled liquid. As the temperature keeps decreasing,

the so-called glass transition occurs at a certain temperature ‘ T_g ’ below which they become glasses. These behaviors are well explained by volume-temperature curve as shown in Fig. 1.4. Glasses are typical examples of materials that exist in metastable and non-equilibrium states which are classified as amorphous materials. Not all of amorphous materials, however, become glasses. Glasses exhibit the following features as an example. Above T_g , viscosity (η) generally varies according to the well-known Vogel-Fulcher law, where η_0 and B are constants.

$$\eta = \eta_0 \exp\left(\frac{B}{T - T_0}\right) \quad (1.1)$$

If $T_0 = 0$, this expression becomes the Arrhenius equation. For the case of $T_0 \neq 0$, the activation energy cannot be defined definitely, namely, its value varies with temperature. This suggests that the activation process cannot be defined uniquely, but that many processes are involved. According to Angell [3], glasses following Arrhenius law are called strong glasses, while those following Vogel-Fulcher law are called fragile glasses [4]. As it is well known, T_g depends on the speed of liquefaction. This means that T_g is not uniquely determined, so that the glass transition is not a phase transition in the usual sense. Amorphous materials like crystalline solids can be insulators, semiconductors, metals, and even superconductor at very low temperature. The present work deals with the amorphous semiconductors.

1.4 Classification and applications of amorphous semiconductors (a-semiconductors)

Amorphous semiconductors, which are constituted mainly from covalent bonds, are classified broadly into two types, i.e., tetrahedrally bonded amorphous semiconductors such as Silicon (Si) and Germanium (Ge) and chalcogenide glasses. Besides single-element materials such as Selenium (Se), Tellurium (Te) and Sulphur (S), chalcogenide glasses are normally constituted from the compounds of chalcogens such as Se, Te, S and other elements such as Arsenic (As), Ge, Indium (In), Tin (Sn), Silver (Ag), Lead (Pb), etc. Typical materials in this classification are listed in Table 1.1. These materials are of particular interest from the view-point of their applications. However, the physics of

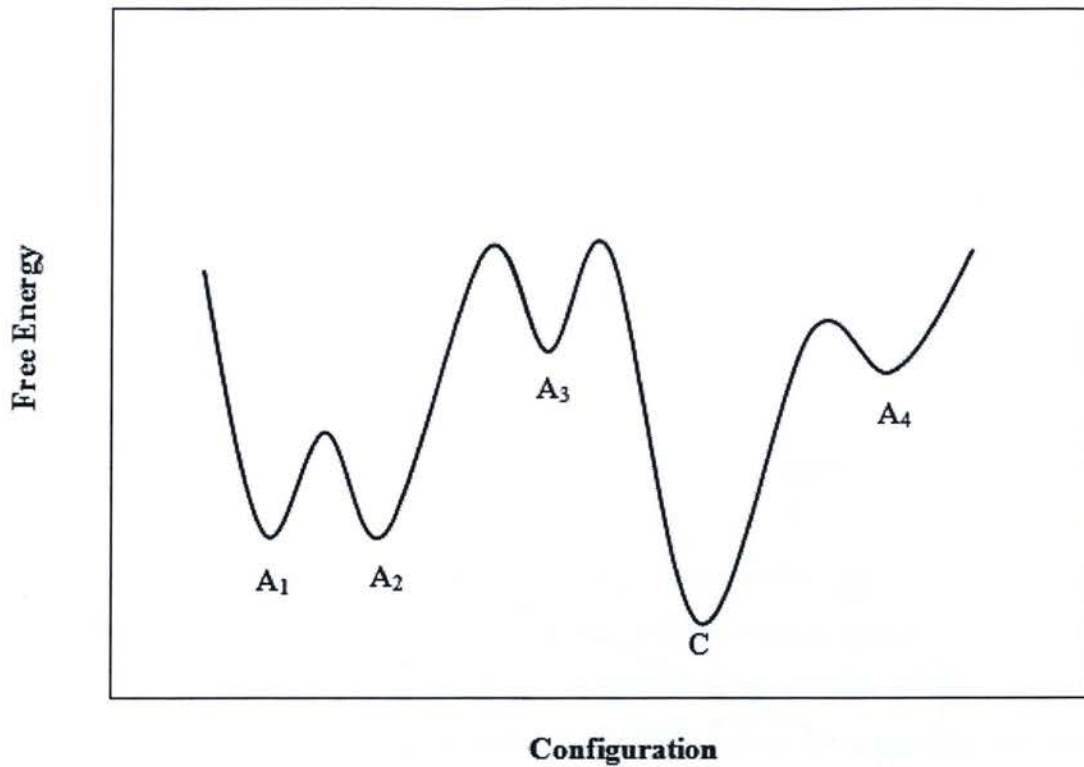


Figure 1.3 Schematic illustration of the free energy versus configuration [Ref. 49]

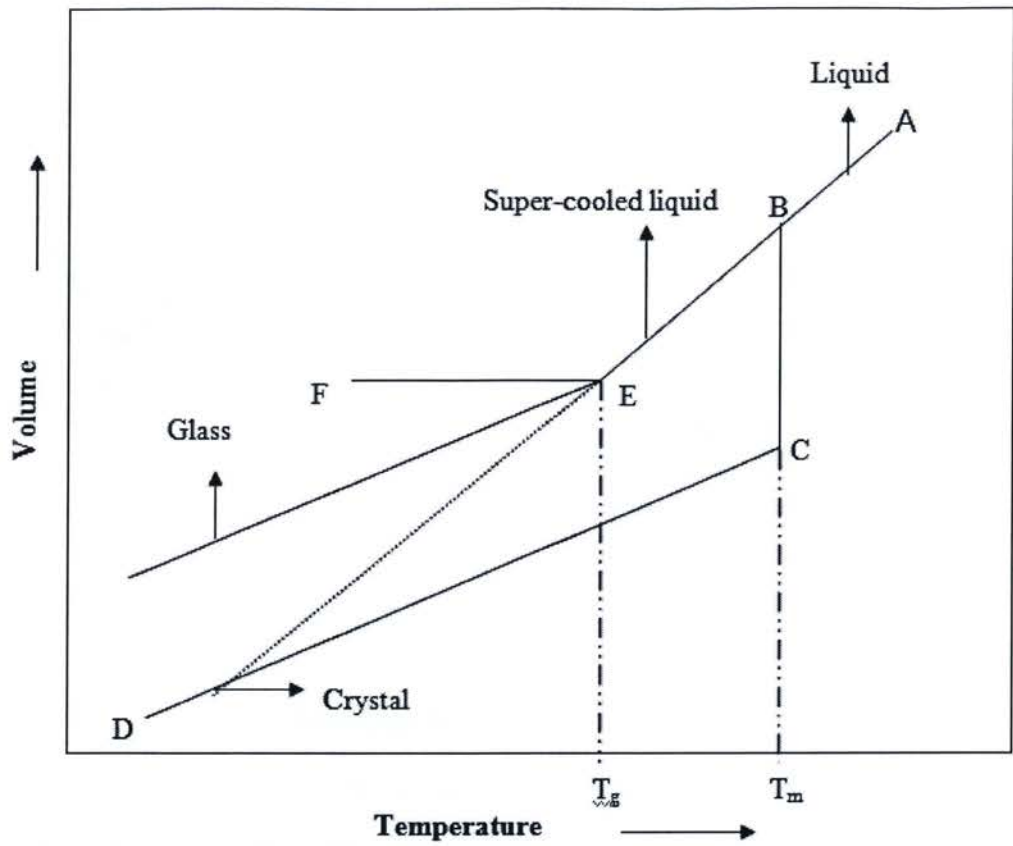


Figure 1.4 Volume versus temperature curve for glass forming systems: T_g : glass transition temperature, T_m : melting temperature [Ref 4]

these disordered systems is not fully established. The tetrahedrally bonded amorphous semiconductors have wide range of applications such as in solar cells, thin film transistors, sensors etc., while chalcogenide semiconductors are the potential candidates for applications in the optical fibers, infrared optical elements, xerography, switching and memory devices [4]. More recently, they have found applications in reversible phase optical recording devices [5-6]. Around 1950 amorphous selenium (a-Se) was investigated as a photoconductor for electro-photography and for photoconductive television picture tubes [7]. This was presumably the first introduction of amorphous semiconductors to device applications.

Amorphous selenium and chalcogenides have been investigated and commercially used since electro-photography was first proposed [7]. The field of amorphous materials has made a significant impact on two of the largest and most fundamental areas of our global economy *information and energy*. The feature that permits amorphous materials to be used in devices for encoding, switching, transmission and storage of information, and also enables the development of new pollution free technology for generation and storage of energy, is the ability to design local atomic order in these materials, free from the conventional constraints imposed by the periodicity of a crystal lattice.

Amorphous semiconductors provide a matrix in which unique physical, electronic, chemical and structural changes can take place. Following design rules, one can make materials in thin film form for example, which can be sensitive to light and provide the basis of the growing field of thin film photo-voltaics. One can design glassy thin film semiconductor materials based on chalcogenide alloys in which the amorphous structure is stable to high field excitation and unique, high speed, reversible electronic switching takes place. These materials are the basis of the Ovonic threshold switch [8]. In the Ovonic memory switch, which is also based on chalcogenide glass alloy, electric field excitation causes a reversible crystalline to amorphous phase change to take place. These materials form the basis for the very successful phase change erasable optical memory disks [8].

There is a huge market demand for low cost, small size rewriteable recording media (such as a DVD-RW) with high densities and high data transfer rates. More recently the chalcogenide materials based recording media have found applications in the Blue-ray

Tetrahedrally Bonded Semiconductors		Chalcogenide Semiconductors			Semiconducting Oxide Glasses
C	InSb	S	As ₂ Se ₃	Ge-Sb-Se	V ₂ O ₅ -P ₂ O ₅
Si	GaAs	Se	As ₂ S ₃	Se-Te-Pb	MnO-Al ₂ O ₃ -SiO ₂
Ge	GaSb	Te	As ₂ Te ₃	Se-Te-Sn	TiO ₂ -B ₂ O ₃ -BaO
	SiC			As-Se-Te	V ₂ O ₅ -PbO-Fe ₂ O ₃

Table 1.1 Classification of amorphous semiconductors [Ref. 4].

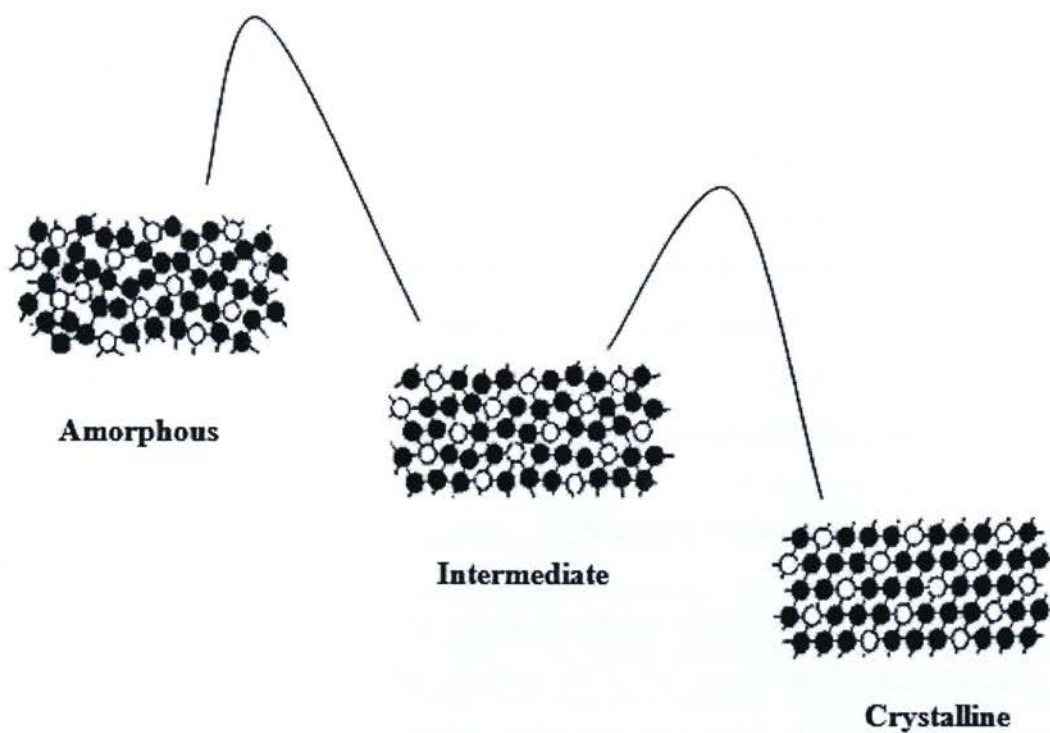


Figure 1.5 Schematic representations of transformations between states with crystalline, intermediate and amorphous atomic structures. The energy barriers between the states can be traversed in either direction by the application of energy pulse profiles [Ref. 8]

discs having storage capacities up-to 50GB, which represents six times the capacity of a dual-layer DVD [9].

Flash memory device manufacturers developing phase change memory are discussing chalcogenide memories as a successor to the current floating gate and nitride storage flash parts beyond the 45nm technology node in applications such as USB keys, digital camera phones, and flash cards. There has been also discussion of using it as a non-volatile RAM in applications such as cell phones which currently use both flash memory and a RAM [10]. Development continues on the chalcogenide switch cell, although test chips have yet to appear.

1.5 Basic physical process

Phase change memories are based on thin film alloys typically incorporating one or more elements from Group VI of the periodic table. These chalcogenide materials can exist in two or more distinct atomic states. An energy barrier must overcome before the structural state can be changed, thereby providing stability in each of the two states. This is shown in Fig. 1.5. Energy can be supplied to the material in various ways, like exposure to laser beam, or by the application of a current pulse. Laser exposure is used for recording, erasing and rewriting in the case of optical memory. If the laser energy supplied exceeds a threshold value, the memory material will be excited to a state of high atomic mobility, in which it becomes possible for the chemical bonding to rapidly rearrange by slight movement of individual atoms. In lone-pair materials, the Group VI atoms use two of their p-electrons to be di-valently bonded, and the atomic rearrangement that takes place during the phase change process may occur by simply shifting the other two non-bonded lone-pair electrons to make new configuration. In order for phase change optical disks to be used in high-speed optical data storage system, the optical memory material must be able to be transformed between the amorphous and the crystalline states using laser pulses of extremely short duration (up to 10^{-6} sec) [7]. At the same time both the states must be stable at room temperature.

1.6 Background on chalcogenide semiconductors

Development of modern technology leads to the appearance of a new family of materials. Among them chalcogenide semiconductors are one of these families due to their interesting properties. Selenium is considered to be one of the most important semiconductors due to its unusual structure [11]. Amorphous semiconductors from Selenium based systems have attracted attention of many researchers. Several studies on thermal and structural properties have been performed on the amorphous selenium obtained by vapor deposition, quenching and ball milling [12-20].

Antimony (Sb) containing chalcogenide glasses have been extensively studied for their interesting electronic and optoelectronic properties [21]. It has been pointed out that addition of Sb to Se improves and stabilizes the amorphous phase [22] and lengthens the crystallization of amorphous selenium [21]. Therefore, Se-Sb based alloy films are thought to be one of the most promising media, which make use of phase change between an amorphous state and crystalline state. Addition of elemental impurities like As, Sn, Bi, Ge, In, Ag, Cu, etc., to Se, Se-Te and Se-Sb causes structural changes in these materials which in turn modifies the band structure and various physical properties like, thermal, electrical and optical properties [23-33]. The increased scientific interest in Se-Sb binary system is due to potential use of Se-Sb thin films in photoconductive elements and as a data storage material [22]. Charge trapping phenomena, transport properties, the relation between the band gap and chemical composition of Se-Sb thin films have been reported in the literature [1, 21-22]. The dielectric studies on Se-Sb based alloys have also been recently reported [4].

A wide variety of light induced changes has been observed in amorphous chalcogenide glasses, ranging from relatively subtle effects involving minor atomic rearrangements and manifested mainly by shifts in optical absorption edge i.e. photodarkening and photobleaching, to more substantial atomic and molecular configurations which causes a variety of physical and chemical changes e.g. photopolymerisation, photocrystallization, photo enhanced dissolution of metals etc. The effects are of interest because of the information they yield on defects and metastable structural states in amorphous solids, and because they are mostly unique to the amorphous state. Review of photoinduced

phenomenon in amorphous chalcogenides has been presented [34], which concluded that the mechanisms responsible for these changes are not fully understood. Photo-induced effects in chalcogenide glasses are of considerable technological importance, having applications in optical imaging, hologram recording and optical memories [35-38].

1.7 Thesis objectives

Chalcogenide glasses and thin films exhibit wide variety of changes in their structural properties, electronic transport and optical properties when they are exposed to light or heavy ion irradiations [39-43]. The structure of amorphous chalcogenide glasses consists of a disordered network having some dangling bonds as defects [4]. When these glasses are irradiated with heavy ions or light, bond breaking and bond rearrangement of atoms takes place, which results in change in local structure order of the amorphous network. Radiation-induced phenomena in chalcogenide glasses are classified into irreversible and reversible ones.

Photoenhanced crystallization, photopolymerization and photodoping are typical examples for the irreversible light-induced phenomenon and on the other hand, reversible light induced phenomenon in chalcogenide glasses has been accounted for in terms of either topological disorder enhanced by illumination or light induced metastable defects. Photodarkening and photostructural change are phenomena caused by topological disorder enhanced by illumination and light induced changes in ac conductivity, photoconductivity, photoluminescence and light induced Electron Spin Resonance (ESR) are phenomena caused by light induced metastable defects [4].

The effect of heavy ion irradiation on the electrical and optical properties of amorphous As-Se thin films has been investigated [40]. It has been concluded from the above studies that ion implantation is a cold method of adding foreign elements to the chalcogenide glasses in such a way that they do not satisfy their valence requirements and thus it is possible to change the energy spectrum of the charged defects states. Influencing, on one hand, the activation energy, which is connected with the Fermi level shift and, on the other hand, the absorption edge, one can conclude that the modification leads to the creation not only of deep but shallow localized states in the gap.

Doping of bulk chalcogenide glassy semiconductors by implanting Ni ions has been reported [41]. It has been observed from the above studies that the ion-induced effect on the Pb-Ge-Se glasses leads to electronic conduction process by a variable range hopping mechanism. Detailed mechanisms describing the effect caused in the chalcogenide glasses by heavy ion irradiation or light illumination are only partially understood. To improve the knowledge about them it is important and necessary to investigate them over a wide range of energy. Although a considerable study of the reversible light-induced phenomena in the chalcogenide glasses have been extensively carried out during the past two decades, the origin of these photo-induced effects is still unclear. Fundamental questions still remain unanswered about the interrelation between the basic characteristics of the photo-structural changes such as red shift in optical band gap, the metastable defect creation process and the photocurrent decay [42].

Chalcogenide glasses and thin films are potential candidates for their various applications such as storage media (for detail see previous section). The addition of elemental impurities to the Se-Sb system modifies the material properties to make it more suitable for the reversible optical recording with an eraser time less than one micro second. Calorimetric studies of Se-Sb-In glasses have been investigated and reported in the literature [21] giving the emphasis on the crystallization and glass transition phenomena at different heating rates. We earlier reported on the "Effect of heavy ion irradiation on the electrical and properties of Se-Sb-In thin films" [43], but not much attention has been given to the photo-induced photo-structural changes in the photocurrent of Se-Sb-In thin films.

The objective of the present thesis is to investigate the steady state and transient photoconductivity measurements of vacuum evaporated amorphous Se-Sb-In thin films. The influence of bias voltage on the dark current and the photocurrent of the thin film samples are studied. The effect of Indium addition to Se-Sb alloy on the dark conductivity, photoconductivity and photosensitivity is also investigated. During the transient measurements the photodegradation in the photocurrent has been observed which has been explained on the basis of charged defect model and inter-cluster interaction model. The behavior of photosensitivity is explained on the basis of chemically ordered network model (CONM) and topological model.

1.8 Thesis outline

In this research we have attempted to analyze the steady state and transient photoconductivity of the thin films of Se-Sb-In system deposited by electron beam evaporation system.

Chapter one presents the introduction of the amorphous chalcogenides. Some literature review of different chalcogenide systems is outlined. The application, importance and objectives of the present study is also presented in this chapter.

In chapter two, some theoretical background and physical models are explained. The methodology to estimate electrical conductivity and optical band gap in the chalcogenide thin films is also given. Chapter three concentrates on the experimental design and methods of measuring the photoconductivity of the thin films is detailed.

The results and discussions are presented in the chapter four of the thesis. The detail explanation of the variation of photocurrent with time supported by charged defect model and inter-chain interaction model. The influence of bias voltage on the dark current and the photocurrent is also reported. The minimum in the dark conductivity, photoconductivity and the photosensitivity at a composition of In = 5 atomic percentage is explained on the basis of chemically ordered network model and the topological model.

Chapter five summarizes the conclusion of the present research and, the scope of future research is also outlined.

Chapter 2

2 Theoretical Background

This chapter describes the theoretical background of amorphous semiconductors. A brief description of defects in chalcogenide glasses is presented. Doping of amorphous chalcogenide is also discussed. In addition, the theory of dc conduction mechanism is given. Determination of the optical band gap from the optical spectra along with the relevant mathematical equations is briefly reviewed.

2.1 Electronic structure and charged defect state models

The knowledge of electronic band structure is required for understanding the electronic properties of materials. In case of crystalline semiconductors, sophisticated theoretical models are presented to understand their band structure. The theoretical understanding of crystalline substance is possible because the periodic crystalline symmetry simplifies the mathematical problems involved in solving the quantum mechanical wave equation. In case of amorphous semiconductors, band structure theories are crude and qualitative because the long-range periodicity is absent. It was first pointed out [44] that the basic electronic properties of amorphous semiconductors are determined primarily by the character of bond between the nearest neighbors rather than by long-range order. It is therefore, as long as the short-range order exists; (in case of amorphous

semiconductors) the main features of electronic band structure are retained. There will be allowed energy bands having non-localized states. The allowed bands will be separated by regions of energy in which localized electronic states exist. The electronic structure of any particular solid depends on the composition, but the general features of the density of states are determined primarily by the predominant form of bonding e.g. tetrahedrally bonded semiconductors, such as germanium and silicon, are characterized by the bonding and anti-bonding bonds near the Fermi energy. On the other hand, if the material contains a large percentage of chalcogen atoms, the presence of so-called high-energy lone-pair electrons leads to qualitatively different electronic energy densities of states, [45], as shown in Fig. 2.1 (a) & (b). The valence band is now non-bonding, and does not contribute significantly to the cohesive energy of the solid [46]. The major difference between the electronic structure of a crystalline and amorphous semiconductor is the possible existence of the tails of localized states in the bands of amorphous semiconductor [47-48]. The understanding of the origin and behavior of the tails of localized states in amorphous semiconductors is the most important. Typical band models suggested for covalent non-crystalline solids in the literature are presented in the sections 2.2 and 2.3 respectively.

2.2 Cohen – Fritzsche - Ovshinsky (CFO) Model

This model assumes that the tail states extend across the mobility gap as shown in Fig. 2.2 (a) which represents the density of states $N(E)$ at the energies corresponding to the valence band (E_V), Fermi level (E_F) and the conduction band (E_C). This model is based on the concept of an ideal covalent random network (CNR), which is realized more closely by the chalcogenide glasses. The compositional and translational disorders are assumed to cause potential fluctuations that give rise to the localized states extending from the conduction and the valence bands into the gap states [49]. Moreover, it is suggested that there should be a sharp boundary between the energy ranges of extended and localized states. The edges, which separate the localized and extended states, are called mobility edges. The gradual decrease in the localized states destroys the sharpness

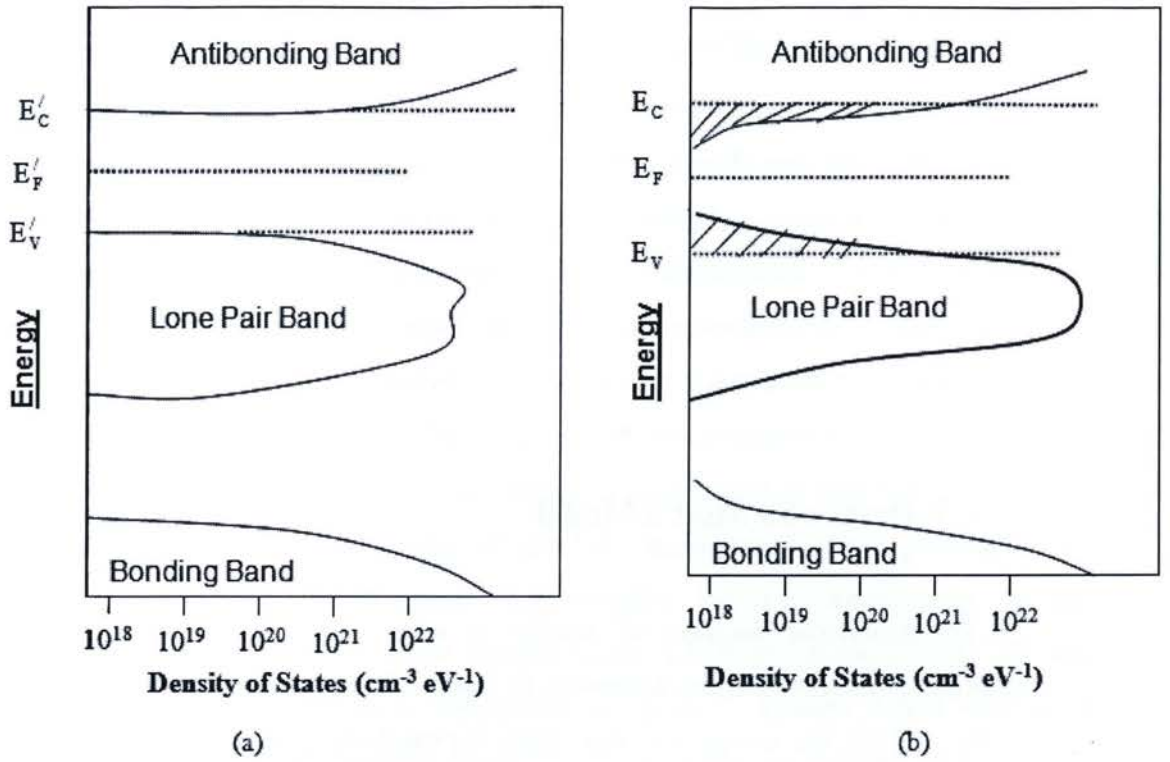


Figure 2.1 Sketch of the electronic density of states of (a) a perfect crystalline chalcogen solid (b) an ideal amorphous chalcogen solid [Ref. 4]

of the conduction and valence band edges. According to this model, in the chalcogenide glassy alloys the disorder is sufficiently high so that the tails of the valence band and conduction bands overlaps, which give rise to appreciable density of states in the middle of the gap. Some of the filled valence band states may have higher energies than states in the conduction band, which are normally empty. Now a redistribution of electrons must takes place, forming filled states in the conduction band, which are negatively charged and the empty states in the valence band, which are positively charged, so that the Fermi-level is pinned close to the middle of the gap, a feature required by the electrical properties of amorphous semiconductors. One limitation of this model is the high transparency of the amorphous chalcogenide below a well-defined absorption edge.

2.3 Davis and Mott's Model

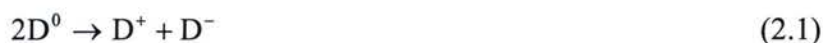
The schematic diagram of density of states $N(E)$ versus band energy (E), for amorphous semiconductors according to Davis-Mott model [50] is shown in Fig. 2.2 (b). In Fig. 2.2 (b), the energy axis represents the band energies corresponding to the valence band (E_V), the Fermi level (E_F) the conduction band (E_C) and the energy (E_A) and (E_B) related to the band edges of conduction band and the valence band. The tails of localized states is narrow and extend only up to a few tenths of electron volt into the forbidden gap. Moreover, there is a band of compensated levels near the middle of gap, originating from defects in random network. It has been suggested that at the transition from extended states to localized states, the mobility drops by several orders of magnitude producing a mobility edge, because the mobility is zero in the localized states at $T= 0K$. The separation between the conduction band mobility edge (E_C) and the valence band mobility edge (E_V) is defined as the mobility gap. The center band may split into two bands, such as, donor band and acceptor band, which will also pin the Fermi level [51] as shown in Fig. 2.2 (c). Marshall et al, 1971 proposal a model with bands of donor and acceptor in the upper and lower halves of the mobility gap. Owen and Spears presented a model for As_2Se_3 [Fig. 2.2 (d)], which shows that the density of states of the glass does not decrease monotonically into the gap, but show many peaks that can be well separated

from each other [52]. The position of the Fermi-Level is largely determined by the charge distribution in the gap states.

2.4 Defect states in the band gap of chalcogenide elements and Compounds

Chalcogenide glasses are diamagnetic in nature and do not show Electron Spin Resonance (ESR) signal, i.e. there appear to be no dangling bonds in the gap. On the other hand the Fermi-level appears to be pinned, suggesting a finite density of gap states. It was largely to resolve this contradiction that models of defect states were first proposed.

The model suggested by Mott, Davis and Street (the so-called MDS model) [53-55] has been successful in explaining a wide variety of phenomena in chalcogenide glasses, such as the constant activation energy of the DC conduction (i.e. the pinning of the Fermi-level), magnetism, luminescence, drift mobility and a.c. conductivity. In this model, bonding defects can have three charged states, which are denoted by D^+ , D^- and D^0 , associated with different local configurations, here D denotes defect state or a dangling bond. The neutral dangling bond D^0 , say a singly coordinated chain-end Se atom, would normally possess spin but it is unstable. Provided the temperature is high enough so that some atomic movement is possible, one of the end atoms move closer to and cross links with the lone-pair p-electrons of a Se atom in a neighboring chain [Figs. 2.3 (a) & (b)]. The three-coordinated Se-atom now gives up an electron to the remaining dangling bond. The former becomes D^+ , the later D^- , and both are now diamagnetic. The reaction



is exothermic because of a negative correlation energy, the potential energy decrease resulting from spin sharing more than compensating the coulomb-repulsive energy increase. The decrease in energy can also be regarded as the result of converting a non-bonding lone pair of electrons into a lower lying σ bonding state by dative bonding. The D^+ and D^- centers lie in the gap and determine the position of the Fermi-level, rather like donors and acceptors in a compensated semiconductor. On a configurational coordinated diagram as shown in Fig. 2.3 (iii), the positive correlation energy 'U' associated with the

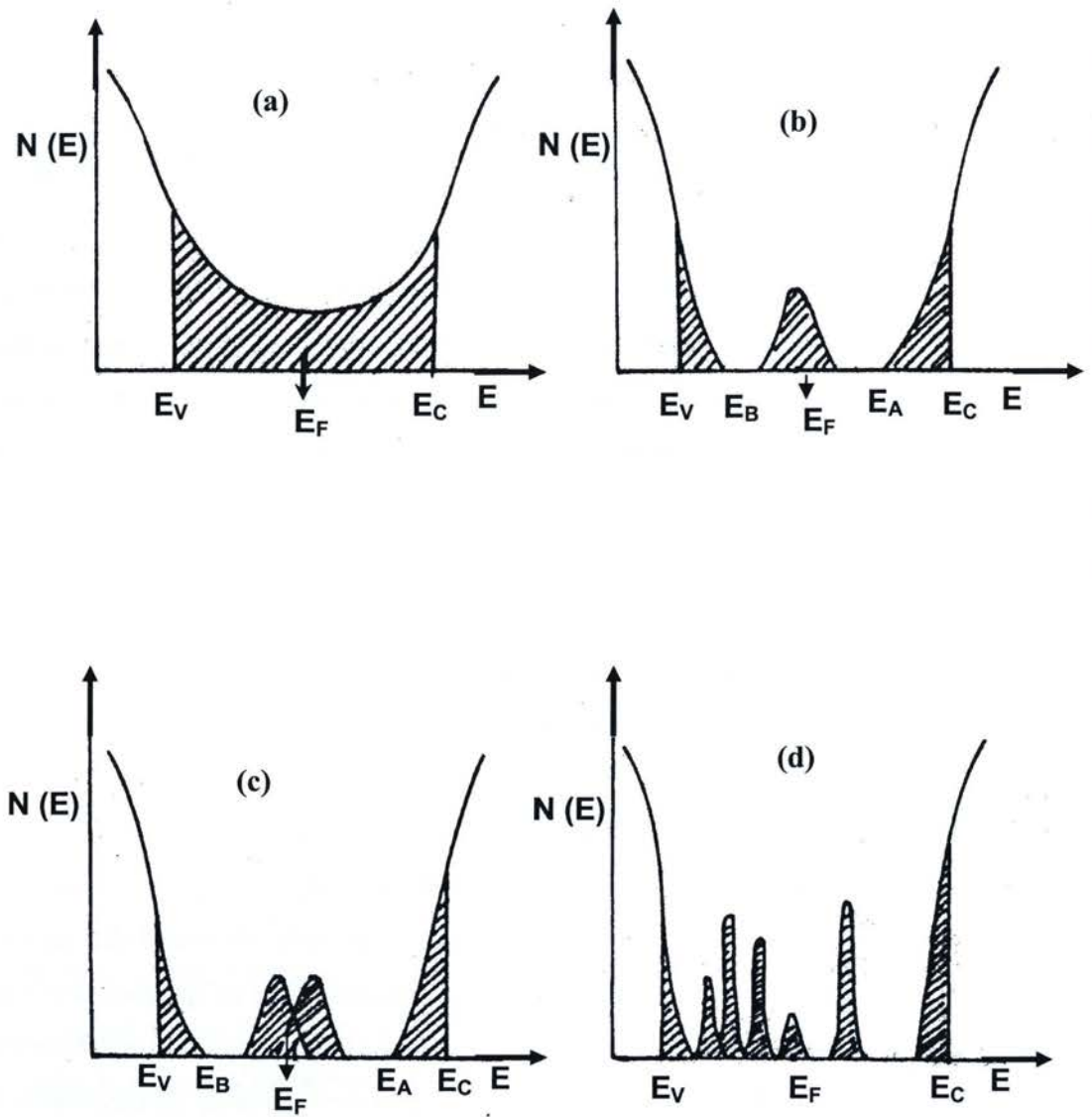


Figure 2.2 The density of states diagrams for amorphous semiconductors in different models: (a) CFO model (b) Davis-Mott model (c) Modified Davis-Mott model (d) A real glass with defect states [Ref. 49].

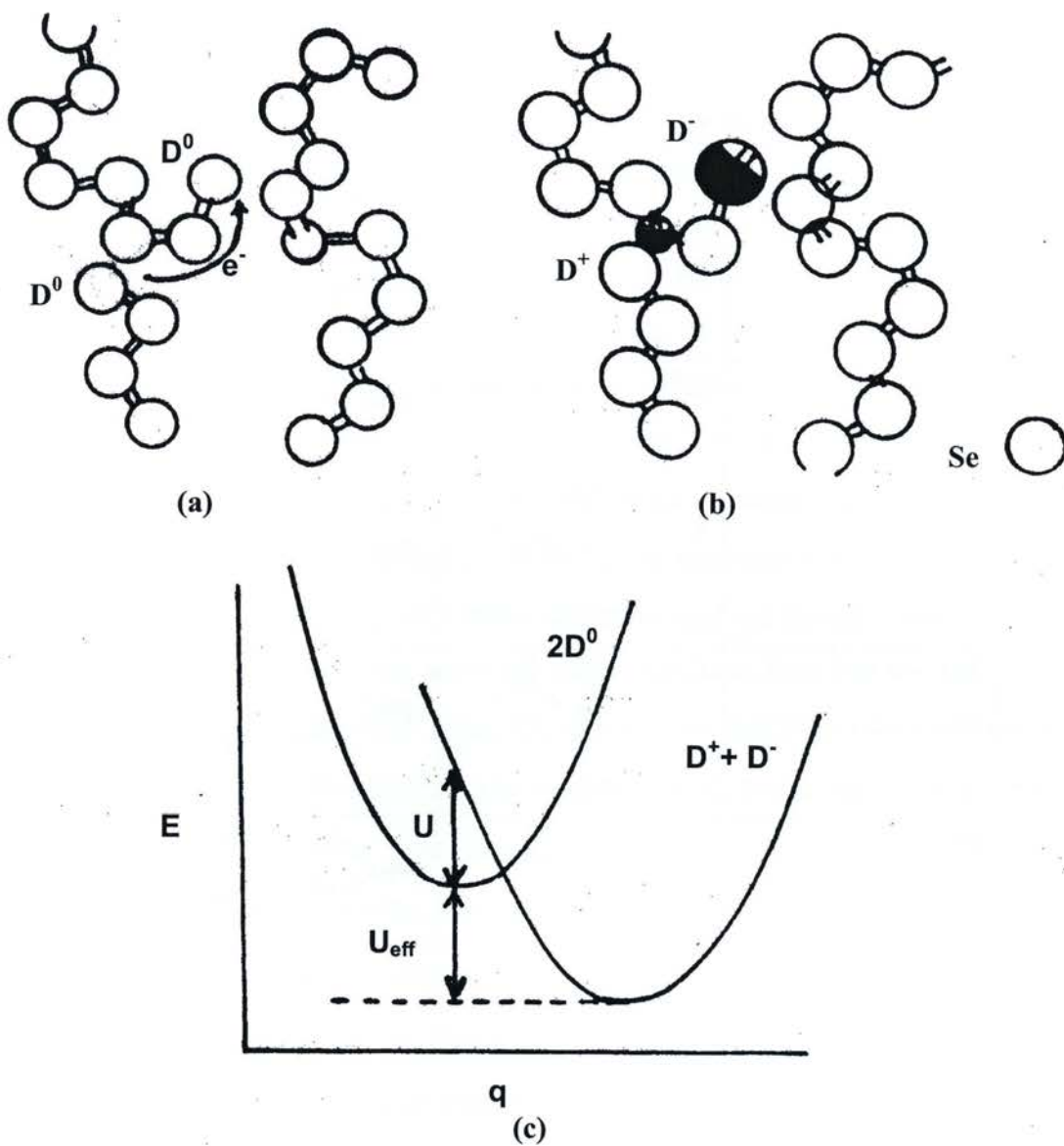


Figure 2.3 (a) and (b) Illustration of the transfer of an electron from one chain end to another creating two charged defects D^+ and D^- (c) The positive correlation energy U associated with two electrons at one site turned into an effective negative correlation energy U_{eff} because of the configurational changes, "q" is configurational coordinate [Ref. 49].

	Configuration		P level occupation	Energy/configuration
(i)	C_2^0	$:\angle$		$-2E_b$
(ii)	C_1^-	$:\text{---}$		$-E_b + U_{Lp}$
(iii)	C_1^0	$:\text{---}$		$-E_b$
(iv)	C_3^-	---		$-E_b + 2\Delta + U\sigma^*$
(v)	C_3^+	---		$-3E_b$
(vi)	C_3^0	---		$-2E_b + \Delta$

Table 2.1 Structure and energy of various defect configurations in a two-fold coordinated material. Arrow represents the spin of electron. In column two, C refers to the chalcogenide atom, the superscript is the charged state and subscript is number of neighbouring atoms [Ref. 44]

-two electrons at D^- in the absence of configurational changes becomes negative (U_{eff}) after lattice relaxation. The configuration coordinate (q) represents a linear combination of the real-space shifts of the intermolecular coordinates from their equilibrium position. The chemical reason for the nature of the reaction is that at D^+ , an extra bond with a neighboring chain can be formed by utilizing the normal non-bonding lone-pair electrons. The coordination of Se atoms at D^+ is, therefore, three, in contrast to that at D^- where it is one and at normally bonded Se atom where it is two. It has been proposed that lattice distortion at D^- is negligible, at D^+ it is considerable and it is intermediate at D^0 . The energies and structures of various simple bonding configurations for a chalcogen, proposed by Kastner and Fritzsche are presented in Table 2.1 [56], according to which, the normal bonding configuration is C_2^0 , here C denotes the chalcogen atom. The straight line is representing bonds (σ - states) and, the dots the lone-pair non-bonding electrons. In this configuration, the anti-bonding (σ^*) states are empty and the energy relative to the lone pair level, is $-2E_b$. Anti-bonding states are pushed up, from lone pair energy; more than bonding states are pushed down. Thus, C_3^0 which is neutral three fold coordinated atom with an extra electron placed in the anti-bonding orbital, has a higher energy than C_2^0 by an amount Δ . The electron in an anti-bonding orbital is represented by (*). The C_3^+ configuration, with energy of $-3E_b$, is the defect having lowest energy. The energy of C_3^- is $-E_b+2\Delta+U_{\sigma^*}$, the positive correlation energy term U_{σ^*} is arising because two electrons are in the anti-bonding state. The extra electron at a normal dangling bond C_1^0 is indistinguishable from the two lone pair electrons at the site and so energy of this defect state is $-E_b$. Finally, a negatively charged dangling bond C_1^- has four electrons in the lone-pair state; its energy is $-E_b + U_{\text{LP}}$, the term (U_{LP}) is energy corresponding to lone pair and arises from the correlation energy in this level. The reaction corresponding to previous equation 2.1 in Kastner's Notation, is as follows



which would be exothermic if

$$-4E_b+2\Delta > -3E_b- E_b+U_{\text{LP}} \text{ i.e., if } 2\Delta > U_{\text{LP}} \quad (2.3)$$

The charged defects C_3^+ and C_1^- have been called by Kastner as a valence alteration pair (VAP). Their creation starting from a fully bonded network, in which all atoms are in the C_2^0 configuration, can be described by the reaction



The above reaction costs energy given by

$$-3E_b - E_b + U_{LP} + 4E_b = U_{LP} \quad (2.5)$$

This is justified as the number of covalent bonds remains unchanged. A high density of such inherent defects is found in many chalcogenide materials. This indicates that the energy of this reaction is relatively small (between 0.5eV – 1.0eV) [57]. VAP's pins the Fermi energy level. The concentration of VAP's present in a sample prepared by cooling from the melt, assuming equilibration at the glass transition temperature T_g , is then $N \exp(-U_{LP}/2kT_g)$, where N is the concentration of lattice sites. For the films deposited onto a substrate at a temperature less than T_g , the concentration might be expected to be lower. The negative correlation energy, which makes the Eq 2.1 exothermic, can also be understood as follows. Let the addition of an electron from the valence band to D^+ state costs an energy E_1 and the addition of an electron to D^0 state costs an energy E_2 , so that,



if the addition of second electron to D^- costs less energy than the first (i.e. $E_2 < E_1$, means the negative correlation energy), then $E_1 - E_2$ is positive and the total reaction is exothermic.

2.5 Doping of amorphous chalcogenide glassy semiconductors

The chalcogenide semiconductors are characterized by Fermi-level pinning. Doping of these glasses has been studied by Kastner and Fritzsche [56]. According to them, the thermal excitation of an electron from C_1^- to the conduction band follows the reaction $C_1^- \rightarrow C_3^0 + e$, and it requires energy E_1 . Removal of second electron from the resulting defect, i.e., $C_3^0 \rightarrow C_3^+ + e$, costs energy E_2 ($E_2 < E_1$). The inter conversion

reaction $C_1^- \rightarrow C_3^+ + 2e$ has reaction energy $2\varepsilon_n = E_1 + E_2$. Thus it takes on the average ε_n to exit one electron to the mobility edge E_c or ε_p to exit a hole to E_v , where $\varepsilon_n + \varepsilon_p = E_g$, the mobility gap. This places the Fermi level at $E_C - E_F$ or $E_F - E_v = \varepsilon_p$. The conductivity activation energy is smaller of the two quantities ε_n and ε_p . There can be two different cases by adding foreign atoms to an amorphous chalcogenide semiconductor depending upon the mode of addition of the additives.

2.5.1 The addition of foreign additive after equilibration

The foreign additive put in the melt of a bulk chalcogenide glass and intrinsic defect states known as Valence Alteration Pairs (VAP's) are allowed to equilibrate by annealing the glass near its T_g . Most of the elements added to the melt of chalcogenide glasses seek lowest energy bonding configuration and thus remain electrically inactive. However, certain elements or fraction of same additives will be incorporated as charged centers. Such centers equilibrate at T_g and yield positive centers of concentration A^+ in case an electropositive additive, which remain fixed below T_g and equilibrate with the total density of VAP's according to the relation,

$$N_0^2 = [C_3^+][C_1^-] = N_A^2 \exp\left[\frac{-E_{VAP}}{kT}\right] \quad (2.9)$$

Here N_A is the density of chalcogenides, k is Boltzmann constant and T is absolute temperature. E_{VAP} is the energy to create a defect pair (VAP) from two normally bonded chalcogen according to the following relation,



It can be shown [4] that in case of electropositive additives, the concentration of free electrons (n), the dopant (A^+) and the neutral charged defects (N_0) are interrelated through following equation

$$n^2 \left[\frac{2N_0}{A^+} + n \right] = 2(A^+)n_0^2 \quad (2.11)$$

where n_0 is the electron concentration defined by the equation

$$n^2 \left(\frac{C_3^+}{C_1^-} \right) = N_c^2 \exp\left[\frac{2\varepsilon_n}{kT}\right] = n_0^2 \quad (2.12)$$

where N_c being the density of band states at conduction band mobility edge. In the case $n \geq \frac{2N_0^2}{A^+}$, the equation 2.11 becomes $n = [2(A^+)]^{\frac{1}{3}} n_0^{\frac{2}{3}}$, which leads to the reduction of the thermal activation energy to 2/3 of its original value, which was predicted by Mott [57]. In the more common case prevailing at ordinary and lower temperature, $n \leq \frac{2N_0}{A^+}$, because N_0 is of the order of 10^{17} cm^{-3} and A^+ is most likely to be less than 10^{21} cm^{-3} , which yields $\frac{2N_0^2}{A^+} \geq 10^{13} \text{ cm}^{-3}$. Equation 2.11 can be rewritten as

$$n = \frac{A^+}{N_0} n_0 \quad (2.13)$$

This means that the activation energy of n retains the value ε_p to ε_n when A^+ is added. This is the case when $\varepsilon_p < \varepsilon_n$. The remarkable property of valence alternation centers to retard the ionization of additive in addition to their ability to increase the density when charged additive occurs strongly reduces the effectiveness of the foreign atoms for altering the conductivity. Since the VAP's concentration N always exceeds A^+ (if a material is allowed to equilibrate), the reaction $C_1^- \Leftrightarrow C_3^+ + 2e$ continues to be the source of electrons with average activation energy ε_n . In order to achieve a more profound modification of electrical properties of chalcogenide it seems necessary, therefore, to prevent equilibrium between the additives and the valence alternation centers.

2.5.2 Non-equilibrium modification of chalcogenides

It is very interesting to note that when the additives leading to charged centers are introduced at sufficiently low temperature so that VAP's concentration 'N' can not change. Such non-equilibrium incorporation may be accomplished, for instance, by field assisted diffusion, co-evaporation or co-sputtering onto a cooler substrate. The value of N and A^+ are then determined by the preparation conditions. As long as $A^+ < N$, the situation is not much different from that described in the last section. When the concentration A^+ exceeds total VAP's concentration N , then the chalcogenide glass

behaves like an ordinary partially compensated semiconductor with A^+ shallow donor, N compensating states in the form of C_1^- and $A^+ - N$ electrons equilibrating with A^+ according to $A^0 \leftrightarrow A^+ + e$. In the hydrogenic model the activation energy E_D of an isolated donor A^0 is related to Rydberg energy by $E_D = \frac{R_m^*}{mk^2}$ which yields $E_D \sim 0.25$ eV for $k = 7.4$ and the effective mass $m^* = m$.

The Fermi-level is then near $E_c - E_F = E_D$, i.e., close to the conduction band and large carrier concentration may be obtained. It is important to note that the bonding configuration of a neutral A^0 center is different from that of a neutral additive A, which has satisfied its bond requirements and which is in its low energy bond configuration. The increase in conductivity and decrease of activation energy were obtained by co-deposition of the transition metal additives and lone pair amorphous semiconductors onto the cold substrate [58]. In the present study doping by incorporation of foreign additives in the melt has been used.

2.6 General conduction mechanism (temperature dependence of DC conductivity)

Accepting the mobility gap idea, four possible mechanisms of conduction may be expected and each will dominate the DC conductivity in an appropriate range of temperature. Starting from high temperatures we describe the four conduction processes as follows [49]:

1. At very high temperature, conduction occurs by carriers excited into the extended states just above E_c (Region A of Fig. 2.4) or just below E_v . In the case of hole transport, for instance, the conductivity is given by following equation:

$$\sigma = \sigma_0 \exp\left[\frac{-(E_F - E_v)}{kT}\right] \quad (2.14)$$

where σ_0 is the pre-exponential factor, k is Boltzman's constant, E_F is the Fermi-level and T is the absolute temperature.

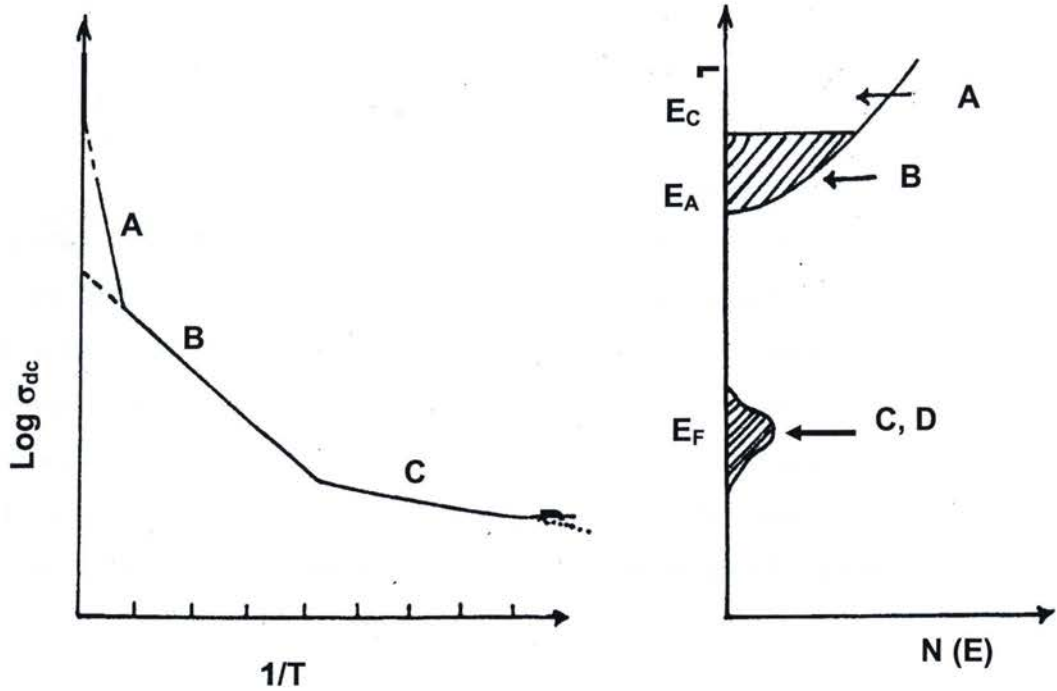


Figure 2.4 Temperature dependence of dc conductivity in a semiconductor on the basis of Davis-Mott model. The regions marked as A, B, C and D corresponds to conduction occurring dominantly at the energies shown on the right [Ref. 49].

Optical measurements usually show that the band gap of amorphous semiconductors decreases approximately linearly with temperature i.e.,

$$(E_F - E_V) = E(0) - \gamma T \quad (2.15)$$

where $E(0)$ is the value of $(E_F - E_V)$ at $T = 0$, the slope will be $E(0)/k$, and the intercept on Y-axis will be $\sigma_0 \exp\left(\frac{\gamma}{k}\right)$.

2. In chalcogenide semiconductor glasses, the temperature coefficient of fundamental absorption edge, which is approximately equal to the mobility gap, is usually found experimentally to be in the range of $4 \times 10^{-4} \text{ eV deg}^{-1}$. Moreover, the Fermi level is situated near the middle of the gap and hence values of γ roughly half that magnitude are to be expected; the magnitude of $\sigma_0 \exp\left(\frac{\gamma}{k}\right)$ is therefore, likely to be in the range of 10-100. The constant σ_0 is generally equated with $\sigma_{\mu\text{iv}}$ the so-called minimum metallic conductivity. $\sigma_{\mu\text{iv}}$ is defined as the smallest non-zero value the conductivity can have at absolute zero degree temperature. i.e. the lowest value of the conductivity contributed by carriers just at E_c (in case of electrons) before the start of activated process. Mott derived the simple relationship $\sigma_{\text{min}} = \text{Const.} \left(\frac{e^2}{ha}\right)$ where a is the inter-atomic distance. The constant h depends somewhat on structure and is in the region 0.03 – 0.1 so that σ_{min} is 200-800 $\text{ohm}^{-1} \text{ cm}^{-1}$, if $a = 3\text{\AA}$. For conduction in extended states therefore the pre-exponential factor, should be roughly $10^3 - 10^4 \text{ ohm}^{-1} \text{ cm}^{-1}$. Transport by carriers excited into the tail of localized states at energies close to E_A or E_B (See region B of Fig. 2.4) and migrating by hopping mechanism, assuming conduction by holes again,

$$\sigma = \sigma_1 \exp\left[\frac{-(E_F - E_B + w_1)}{kT}\right] \quad (2.16)$$

where w_1 is the activation energy for hopping, and E_B is the energy at the band edge. It is not easy to make estimate of the pre-exponential factor, σ_1 , but the lower mobility and the lower density of states near E_B compared with E_V , will

make it several decades smaller than σ_0 . The energy difference $E_F - E_B$, is also expected to depend upon temperature but that is still difficult to determine. The quantity k in Eq. 2.16 is the Boltzmann constant and T is the absolute temperature.

3. At lower temperatures a significant number of carriers is not excited but if the density of states at the Fermi-level is finite there will be a contribution from carriers with energies near E_F hopping between localizes states (See region C of Fig. 2.4). In this case,

$$\sigma = \sigma_2 \exp\left[\frac{-W_2}{kT}\right] \quad (2.17)$$

where W_2 is the appropriate hopping energy and $\sigma_2 < \sigma_1$.

4. At still lower temperatures it is possible that carriers will tend to hop beyond their spatially nearest neighbor states to states which are closer energetically (See region D of Fig 2.4). This is the so-called variable range hopping mechanism and it has been showed that if the density of states at E_F is $N(E_F)$, then,

$$\sigma = \sigma_3 \exp\left[-\left(\frac{T_0}{T}\right)^{\frac{1}{4}}\right] \quad (2.18)$$

$$\text{with } T_0 \approx \frac{\lambda \alpha^3}{kN(E_F)}$$

where α is the decay constant of the wave function of localized states near E_F ($\sim 10^7 \text{ cm}^{-1}$), λ is the dimensional constant (~ 18), σ_3 is the pre exponential factor of equation 2.18 and k is Boltzmann constant.

2.7 Absorption edge of amorphous chalcogenide semiconductors

Electronic transition between the valence and conduction bands in the crystal start at the absorption edge, which corresponds to the minimum energy difference E_g between the lowest minimum of the conduction band and the highest maximum of the valence band. If these extrema lie at the same point of k -space, the transitions are called direct. If this is not the case, the transitions are possible only when phonon-assisted are called indirect. The rule governing these transitions is the conservation of quasi-momentum during the transition,

either of the electron alone in direct transitions, or the sum of electron and phonon quasi-momenta in indirect transitions. The value of the gap E_g depends in a rather subtle way on the structure and actual values of pseudo-potential in the crystal. It is to be distinguished from the gap E_g , which is the characteristics of the whole absorption and is connected with the basic chemical properties of materials. When the semiconductor becomes amorphous, one observes a shift of the absorption edge either towards lower or higher energies. There is no simple general rule, governing these changes has been suggested. The shape of the absorption edge in most of the amorphous semiconductors is shown in Fig. 2.5. One can distinguish the high absorption region A ($\alpha > 10^4 \text{ cm}^{-1}$), the exponential part B which extends over four order of magnitude of α and the weak absorption tail C.

2.7.1 High absorption region

The high absorption region is shown in part A of Fig. 2.5 (a). It is often observed in semiconducting glasses that, at high enough absorption levels ($\alpha > 10^4 \text{ cm}^{-1}$), the absorption constant α has the following frequency dependence:

$$\hbar\nu\alpha(\nu) \sim (\hbar\nu - E_g^{opt})^r \quad (2.19)$$

where r is a constant and it lies between one to three. The optical transition in amorphous semiconductors has been explained on the basis of a model. The basic difference between amorphous and crystalline semiconductors is the non-conservation of the k -vector. This is due to the change in the character of the wave-functions, some of which becomes localized over a certain volume $V(E)$ rather than extended over the whole volume of the samples as in crystals. When the wave functions are localized, the transition probabilities between the states localized at different sites are reduced by a factor depending on the overlap of the wave functions of the initial and final states.

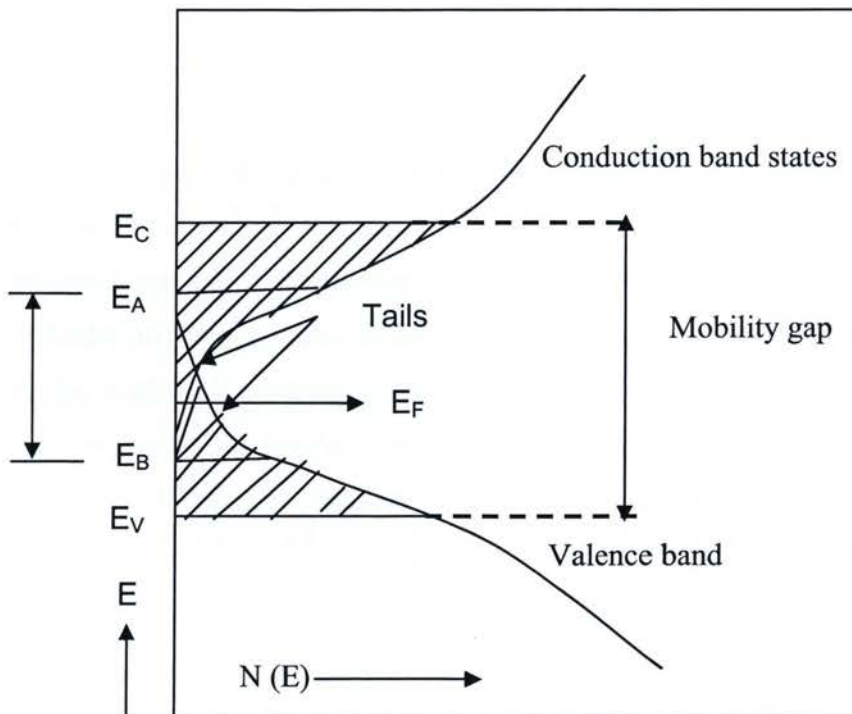
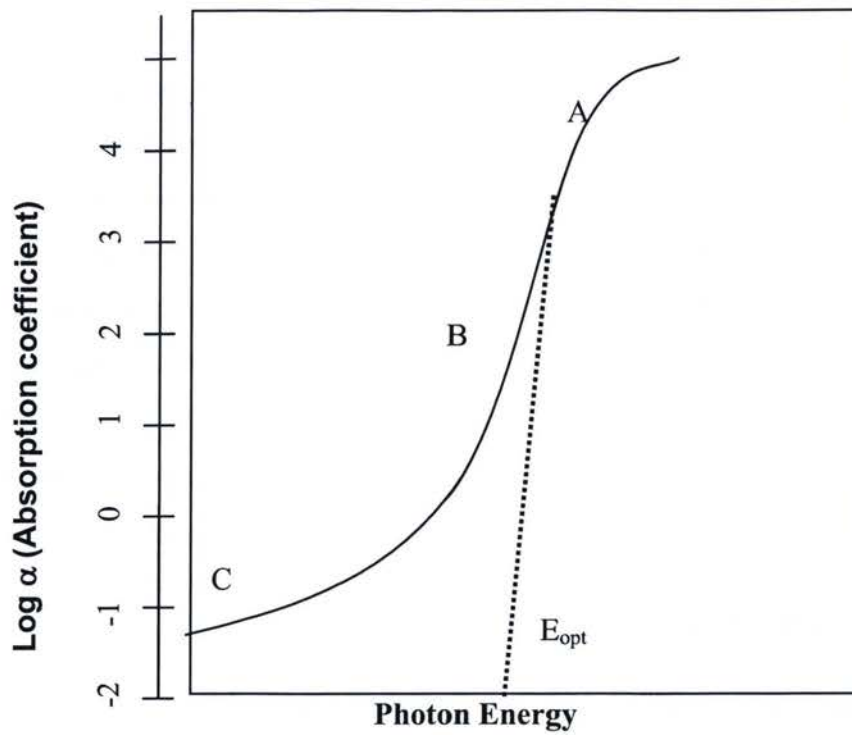


Figure 2.5 (a) Absorption edge in amorphous semiconductors (b) Density of states $N(E)$ as a function of energy E in amorphous semiconductors [Ref. 61].

We consider only transitions between states, of which one is localized and other is extended, or of which both are weakly localized so that the overlapping of the wave function is large enough. Under these circumstances the absorption coefficient α is given by the following equation:

$$\alpha = \frac{2\pi^2 e^2}{m^2 c \nu n} \rho^2 \int V(E) g_i(E) g_f(\hbar\omega + E) dE \quad (2.20)$$

where n is the refractive index, g_i and g_f are the densities of initial and final states. The optical matrix element ρ was assumed to be constant. Rest of the symbols has their usual meanings.

The density of states g_i and g_f are shown in Fig. 2.5 (b). The model of state densities is usually denoted as Mott-CFO model. Part A of the absorption curve is probably associated with the transitions from the localized valence band states in the valence band below E_v into the de-localized states in the conduction band states above E_c^m , or vice-versa and the quantity (E_g^{opt}), is known as optical band gap and is given by,

$$E_g^{opt} = E_c - E_v \quad (2.21)$$

The constant A in the empirical relation

$$\alpha \hbar\nu = A(\hbar\nu - E_g^{opt})^2 \quad (2.22)$$

lies between 10^5 to 10^6 $\text{cm}^{-1} \text{eV}^{-1}$ [59] and the term ($\hbar\nu$) is the energy which is calculated from the wavelength. In this interpretation we determine E_g^{opt} from an extrapolation of the densities of states deeper in the bands.

2.7.2 Exponential region of the absorption edge

The exponential region of the fundamental absorption edge is also termed as Urbach's edge or Urbach's tail [See region B of Fig. 2.5 (a)]. The exponential part of the absorption edge is considered to be due to the transitions between the localized tail states adjacent to the valence band and the extended states in the conduction band above E_c^m ($\hbar\nu < E_g^{opt}$). The absorption coefficient α lies up to 10^4 cm^{-1} in this region. The

frequency and temperature dependence of the Urbach's edge can be described by the following equation

$$\alpha(h\nu) = \alpha_0 \exp\left(\frac{h\nu - E_g^{\text{opt}}(T)}{kT^*}\right) \quad (2.23)$$

where $E_g^{\text{opt}}(T)$ is the temperature dependent gap [$h\nu < E_g^{\text{opt}}(T)$] and is equal to the approximate energy at which absorption coefficient at edge is maximum. The parameter $\Delta = kT^*$ is a measure of the steepness of the exponential tail. T^* is an effective temperature related to the temperature T of the specimen. It is approximately constant at low temperature and proportional to T at higher temperature [60]. The relation in the equation 2.23 is known as Urbach's rule. The value of Δ in many semiconducting glasses lies between 0.05 to 0.08eV and can be determined from the experimental plot using the relation $\Delta = \frac{-d(h\nu)}{d(\ln\alpha)}$.

The crystalline semiconductors also exhibit the Urbach's exponential tail in the absorption edge.

2.7.3 Weak absorption tail

The region below the exponential part of the absorption edge corresponds to the weak absorption tail region [Part C in Fig 2.5 (a)]. Its strength and shape depends upon method of preparation, purity, defect states and the thermal history of the amorphous semiconductors, It is, of course, difficult to study this absorption in thin films because low absorption level. The value of α belongs to this part of the spectrum has been found to be less than 0.5 cm^{-1} [61]. This part of the absorption spectrum is generally interpreted due to the transitions involving (a) both the initial and final states as localized states and (b) the initial localized and final de-localized states.

Chapter 3

3 Explanation of Experimental Set-up Used to Obtain the Analysed Data

The experiments explained in this chapter were previously performed and they are not a part of the objectives of this thesis, however, the data obtained by this experimental set-up have been used in this work. This chapter includes the description of experimental methods/techniques such as X-ray diffraction (XRD), Rutherford back scattering (RBS), and electrical conductivity and optical band gap measurements to characterize the thin film samples. In addition, the design employed to perform studies of the photo-induced phenomenon of Se-Sb-In thin films is presented in this chapter.

3.1 Preparation of bulk samples

Bulk samples of all the different compositions of $\text{Se}_{90-x}\text{Sb}_{10}\text{In}_x$ ($0 \leq x \leq 15$), were prepared by conventional melt quenching technique [1]. High purity elements with 5N purity obtained from Sigma – Aldrich USA were used for the synthesis of the bulk samples. The elements in appropriate amounts were sealed in a quartz ampoule in a dynamic vacuum of the order of 10^{-5} mbar. Three gram of total weight was taken for each set of composition. The composition and weight calculations for bulk $\text{Se}_{90-x}\text{Sb}_{10}\text{In}_x$ ($0 \leq x \leq 15$) samples are given in sections 3.1.1 to 3.1.4 respectively.

The ampoule was placed in a vertical furnace at 830°C for about 48 hours. The temperature of the furnace was increased in the steps of 100°C per hour. The ampoule was frequently inverted in order to ensure the homogeneous mixing of the constituents.

After 48 hours the ampoule was rapidly quenched in an ice mixed water bath. The material was separated from the ampoule by dissolving it into a solution of hydrogen peroxide and hydrofluoric acid ($\text{H}_2\text{O}_2 + \text{HF}$) for about 24 hours.

3.1.1 Weight calculations for 3 grams of $\text{Se}_{90}\text{Sb}_{10}$ composition

Atomic Weight of Se = $A_{\text{Se}} = 78.96$, Atomic Weight of Sb = $A_{\text{Sb}} = 121.75$

Weight calculations for Se_{90}

$$\frac{\text{atomic \% of Se} \times A_{\text{Se}} \times 3}{\text{atomic \% of Se} \times A_{\text{Se}} + \text{atomic \% of Sb} \times A_{\text{Sb}}} = \frac{90 \times 78.96 \times 3}{90 \times 78.96 + 121.75 \times 10} = 2.560\text{g}$$

Weight calculations for Sb_{10}

$$\frac{\text{atomic \% of Sb} \times A_{\text{Sb}} \times 3}{\text{atomic \% of Se} \times A_{\text{Se}} + \text{atomic \% of Sb} \times A_{\text{Sb}}} = \frac{10 \times 121.75 \times 3}{90 \times 78.96 + 121.75 \times 10} = 0.440\text{g}$$

Total weight of $\text{Se}_{90}\text{Sb}_{10}$ composition

= Calculated weight of Se_{90} + Calculated weight of Sb_{10} = $2.560 + 0.44 = 3.0\text{g}$

3.1.2 Weight calculations for 3 grams of $\text{Se}_{85}\text{Sb}_{10}\text{In}_5$ composition

Atomic Weight of Se = $A_{\text{Se}} = 78.96$, Atomic Weight of Sb = $A_{\text{Sb}} = 121.75$

Atomic Weight of In = $A_{\text{In}} = 114.82$

Weight calculations for Se_{85}

$$\frac{\text{atomic \% of Se} \times A_{\text{Se}} \times 3}{\text{atomic \% of Se} \times A_{\text{Se}} + \text{atomic \% of Sb} \times A_{\text{Sb}} + \text{atomic \% of In} \times A_{\text{In}}} = \frac{85 \times 78.96 \times 3}{85 \times 78.96 + 121.75 \times 10 + 114.82 \times 5} = 2.370\text{g}$$

Weight calculations for Sb₁₀

$$\frac{\text{atomic \% of Sb} \times A_{Sb} \times 3}{\text{atomic \% of Se} \times A_{Se} + \text{atomic \% of Sb} \times A_{Sb} + \text{atomic \% of In} \times A_{In}}$$
$$= \frac{10 \times 121.75 \times 3}{85 \times 78.96 + 10 \times 121.75 + 5 \times 114.82} = 0.430\text{g}$$

Weight calculations for In₅

$$\frac{\text{atomic \% of In} \times A_{In} \times 3}{\text{atomic \% of Se} \times A_{Se} + \text{atomic \% of Sb} \times A_{Sb} + \text{atomic \% of In} \times A_{In}}$$
$$= \frac{5 \times 114.82 \times 3}{85 \times 78.96 + 10 \times 121.75 + 5 \times 114.82} = 0.200\text{g}$$

Total weight of Se₈₅Sb₁₀In₅ composition:

= Calculated weight of Se₈₅ + Calculated weight of Sb₁₀ + Calculated Weight of In₅

$$= 2.370 + 0.430 + 0.200 = 3.0\text{g}$$

3.1.3 Weight calculations for 3 grams of Se₈₀Sb₁₀In₁₀ composition

Weight calculations for Se₈₀

$$\frac{\text{atomic \% of Se} \times A_{Se} \times 3}{\text{atomic \% of Se} \times A_{Se} + \text{atomic \% of Sb} \times A_{Sb} + \text{atomic \% of In} \times A_{In}}$$
$$= \frac{80 \times 78.96 \times 3}{80 \times 78.96 + 10 \times 121.75 + 10 \times 114.82} = 2.180\text{g}$$

Weight calculations for Sb₁₀

$$\frac{\text{atomic \% of Sb} \times A_{Sb} \times 3}{\text{atomic \% of Se} \times A_{Se} + \text{atomic \% of Sb} \times A_{Sb} + \text{atomic \% of In} \times A_{In}}$$
$$= \frac{10 \times 121.75 \times 3}{80 \times 78.96 + 10 \times 121.75 + 10 \times 114.82} = 0.420\text{g}$$

Weight calculations for In₁₀

$$\frac{\text{atomic \% of In} \times A_{In} \times 3}{\text{atomic \% of Se} \times A_{Se} + \text{atomic \% of Sb} \times A_{Sb} + \text{atomic \% of In} \times A_{In}}$$
$$= \frac{10 \times 114.82 \times 3}{80 \times 78.96 + 10 \times 121.75 + 10 \times 114.82} = 0.400\text{g}$$

Total weight of Se₈₅Sb₁₀In₁₀ composition:

= Calculated weight of Se₈₀ + Calculated weight of Sb₁₀ + Calculated Weight of In₁₀

$$= 2.180 + 0.420 + 0.400 = 3.0\text{g}$$

3.1.4 Weight calculations for 3 grams of Se₇₅Sb₁₀In₁₅ composition

Weight calculations for Se₈₀

$$\frac{\text{atomic \% of Se} \times A_{Se} \times 3}{\text{atomic \% of Se} \times A_{Se} + \text{atomic \% of Sb} \times A_{Sb} + \text{atomic \% of In} \times A_{In}}$$
$$= \frac{75 \times 78.96 \times 3}{75 \times 78.96 + 10 \times 121.75 + 15 \times 114.82} = 2.0\text{g}$$

Weight calculations for Sb₁₀

$$\frac{\text{atomic \% of Sb} \times A_{Sb} \times 3}{\text{atomic \% of Se} \times A_{Se} + \text{atomic \% of Sb} \times A_{Sb} + \text{atomic \% of In} \times A_{In}}$$
$$= \frac{10 \times 121.75 \times 3}{75 \times 78.96 + 10 \times 121.75 + 15 \times 114.82} = 0.410\text{g}$$

Weight calculations for In₁₅

$$\frac{\text{atomic \% of In} \times A_{In} \times 3}{\text{atomic \% of Se} \times A_{Se} + \text{atomic \% of Sb} \times A_{Sb} + \text{atomic \% of In} \times A_{In}}$$

$$= \frac{15 \times 114.82 \times 3}{75 \times 78.96 + 10 \times 121.75 + 15 \times 114.82} = 0.590\text{g}$$

Total weight of $\text{Se}_{75}\text{Sb}_{10}\text{In}_{15}$ composition:

= Calculated weight of Se_{75} + Calculated weight of Sb_{10} + Calculated Weight of In_{15}

= 2.180 + 0.420 + 0.580 = 3.0g

3.2 Preparation of thin films

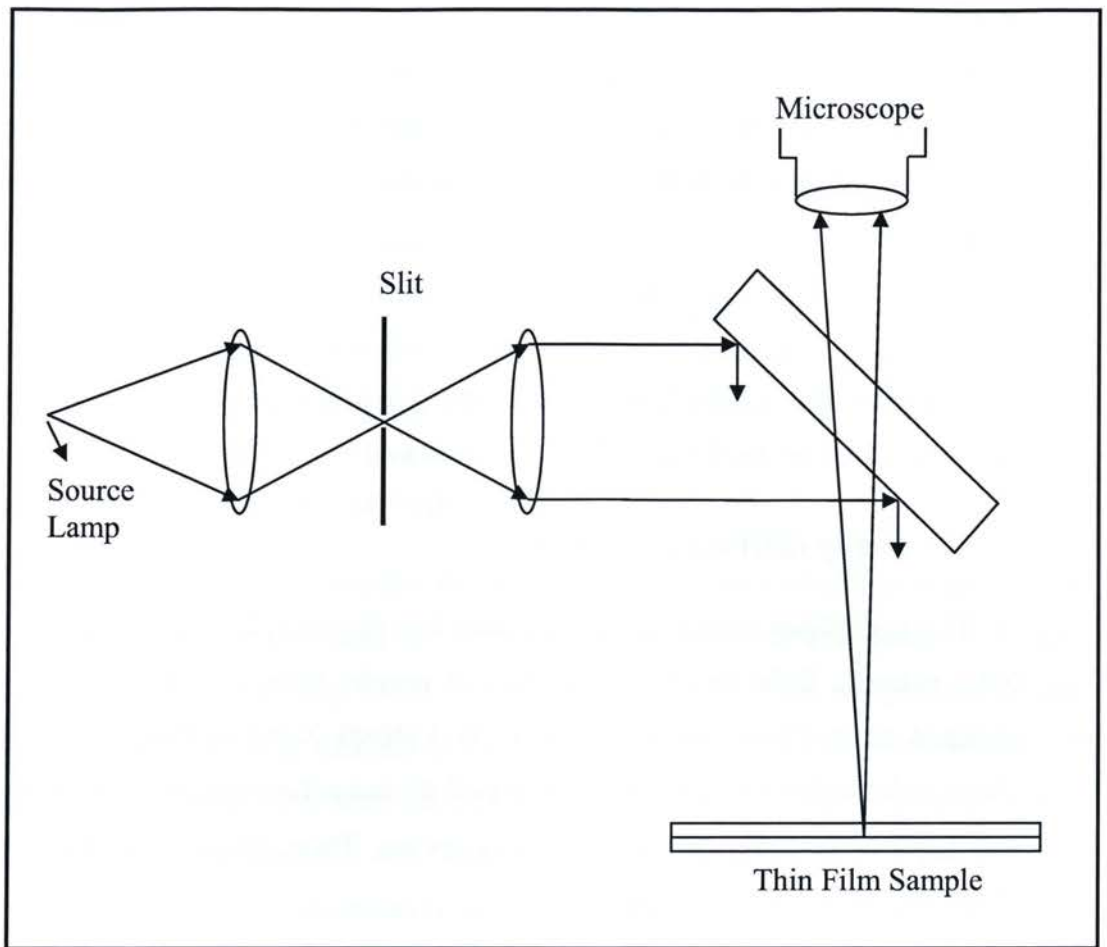
To deposit the thin films, glass substrates were chemically and ultrasonically cleaned. The inorganic impurities from the glass substrates were removed by using the 'aqua regia' solution (A mixture of one part by volume of concentrated nitric acid and three parts of concentrated hydrochloric acid) and the organic impurities were removed by cleaning the slides with liquid soap and distilled water. Thin films from the bulk samples were deposited at room temperature on well-cleaned glass substrates and by electron beam evaporation for $\text{Se}_{90-x}\text{Sb}_{10}\text{In}_x$ ($0 \leq x \leq 15$) samples in a vacuum better than 10^{-5} mbar using HINDHIVAC coating unit (Model 12A 4D). The evaporation rate was kept constant at 10-20 Å per second.

3.2.1 Thickness measurements of thin films

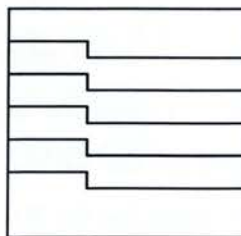
Thickness of the films was measured by Tolansky's interference method [62] and it lies between 2100Å to 3750Å as shown in Table 3.1. The Tolansky's method for the measurement of the thickness of thin films by multiple-beam interference techniques is commonly used to determine the thickness of thin films. Briefly, the film, the thickness of which is to be measured, is deposited on a flat, smooth substrate. The film should have a sharp edge so that a step is formed when the film and the adjacent substrate are coated with an opaque, highly reflecting metallic layer (Aluminum in present case). The height of this step was measured by using the highly reflecting layer as one surface of an interferometer and viewing the multiple-beam fringe system by reflection. Provided that-

Sample	Thickness (Å)
x = 0	2250
x = 5	3750
x = 10	2600
x = 15	2100

Table 3.1 Thickness of $\text{Se}_{90-x}\text{Sb}_{10}\text{In}_x$ ($0 \leq x \leq 15$) thin films measured by Tolansky's method



(a)



(b)

Figure 3.1 (a) Thickness measurement setup (b) Pattern of fringes with the step

the over-layer assumes the exact contour of the surface, this step-height will give the thickness of the film underneath. The typical thickness measurement set up with monochromatic source of light (Na lamp in present case) is shown in Fig. 3.1 (a). The fringe pattern along with the step height is also shown in Fig. 3.1 (b) In order to verify the uniformity of the thin films, the thickness measurements were carried at the different parts of each thin film sample. The relation used to find the thickness of the thin films is given in [4]:

$$t = \frac{h}{w} \times \frac{\lambda}{2} \quad (3.1)$$

Here (t) is thickness of the thin film, (h) is the step height, (w) is the fringe width between two consecutive bright fringes and (λ) is the wavelength of light (5896 Å for Na).

3.3 X-ray diffraction (XRD)

The amorphous nature of the bulk and thin film samples was ascertained by using XRD patterns. Bulk samples were taken in powder form for XRD. XRD pattern was obtained using Cu-K α radiations from PW-1140/09 X-ray diffractometer. Absence of sharp peaks in the XRD spectrum confirmed the amorphous nature of the bulk as well as thin films of Se_{90-x}Sb₁₀In_x (0 ≤ x ≤ 15) system. These spectrum are presented in the chapter 4, section 4.1 of the thesis.

3.4 Rutherford backscattering (RBS)

The composition of thin films of Se_{90-x}Sb₁₀In_x (0 ≤ x ≤ 15) samples was determined by using RBS available at Nuclear Science Centre (NSC) New Delhi, India. The general purpose scattering chamber (GPSC) used for the RBS experiment. The samples were mounted on a target holder inside the GPSC. The films were irradiated at room temperature with 40 MeV Si ion beam for the RBS experiment. A Silicon surface barrier detector (having a depletion depth of 60 μm) was used at back angle of 120° to detect the Si ions back scattered from the sample. Since the masses of the constituents (Se, In, Sb) are quite apart, the back-scattered Si ion appears in three groups well separated from each other, representing three different masses. The area of the peaks and the Rutherford scattering cross section were used to determine the relative composition of Se, In and Sb.

The composition was determined at different parts of the films and was found to be uniform.

3.5 DC conductivity and photoconductivity

The dc electrical conductivity measurements were carried out for thin films in the temperature range 213-313K. Electrical contacts (with electrode gap 1-2mm) in coplanar geometry were made using silver paint. The straight line passing through the origin of the voltage-current plot verified the Ohmic nature of the contacts. The current was recorded by using a digital picoammeter (DPM-111 Scientific Equipments, Roorkee). All the measurements were carried out in a dynamic vacuum of the order of 10^{-5} mbar.

3.5.1 DC conductivity set-up

The sample holder used to mount the samples is shown in a schematic diagram (Fig 3.2). It consists of a copper base, on which thin film sample was mounted. A Pt-100 thermocouple was placed very close to the sample to record the temperature of the sample. A micro-heater was attached to the copper base plate to vary the temperature of the sample. Thin copper wires were used as leads of electrodes, which were connected to the electrodes with silver paint in order to make a good electrical contact. Liquid nitrogen was used as coolant for low temperature conductivity measurements. The dc conductivity of the films was calculated by using following relationship:

$$\sigma_{dc} = \frac{\ell \times I}{A \times V} \Omega^{-1} \text{cm}^{-1} \quad (3.1)$$

where ℓ is the electrode gap, A is the area of cross section and is given as $A = t \times w$, t is thickness and w is the width of the thin film respectively, ' I ' is the current flowing through the sample and ' V ' is the voltage applied to the electrode of the samples.

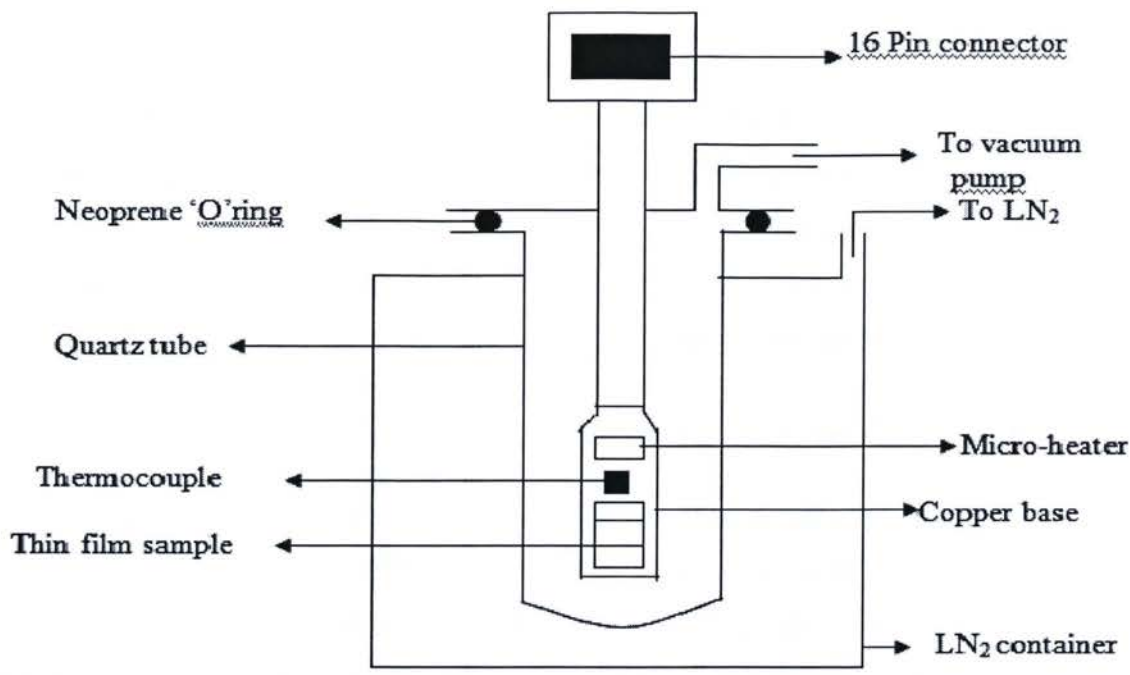


Figure 3.2 Schematic diagram of the dc conductivity and photoconductivity set-up

3.5.2 Photoconductivity

For photoconductivity, thin films samples of $1 \times 2 \text{ cm}^2$ were mounted on a specially designed metallic cryostat with a transparent window inside the vacuum coating unit.. Both the steady state and transient photocurrent measurements were performed in a vacuum of the order of 10^{-5} mbar. A tungsten halogen lamp (Halonix) of 500 Watts was used for illuminating the samples. The IR part of the light was cut off using IR filters. The intensity of the light was measured by using a digital lux meter, (Lx-102, Lutron, Taiwan). A digital picoammeter (DPM-111 Scientific Equipments, Roorkee) was used to record the photocurrent.

The steady state photoconductivity was measured by exposing the thin film samples to light and the photocurrent was recorded once the steady state was reached i.e the photocurrent became constant. Different illumination intensities of light ranging from 500 lx to 5000 lx were used to record the steady state photocurrent at room temperature.

The transient photoconductivity was studied by exposing the thin film samples to light and recording the photocurrent in the time steps (5 sec in present case) until the photocurrent attained a steady state value. The transient photoconductivity of the thin film samples was measured at different illumination intensities of light (500 lx to 5000 lx) at room temperature.

3.6 Optical spectra

The optical transmission spectrum of the thin films was recorded using a UV/Visible spectrophotometer (Shimadzu Japan) at room temperature in the wave-length range 350-1100 nm. The absorption coefficient α is calculated, neglecting the reflection and interference effects using the following relation

$$\alpha = \left(\frac{1}{t} \right) \left[\ln \left(\frac{100}{T} \right) \right] \quad (3.2)$$

where T is percentage transmission and t is the thickness of the films. The intercept of a linear fit of the linear part of the plot of $(\alpha hv)^{1/2}$ versus (hv) on the energy axis (x-axis) gave the optical band gap (E_g) [43].

Chapter 4

4 Results and Discussion

The bulk samples of $\text{Se}_{90-x}\text{Sb}_{10}\text{In}_x$ ($0 \leq x \leq 15$) were prepared by the melt quenching technique as described in chapter 3. In this chapter the structure and the photoelectric properties (steady state and transient) of $\text{Se}_{90-x}\text{Sb}_{10}\text{In}_x$ ($0 \leq x \leq 15$) system have been included. The photodegradation in the photocurrent has been observed upon the illumination with light. The decrease in the photocurrent was explained on the basis of charged defect model and the inter-cluster interaction model. The photosensitivity studies are also carried out and results were discussed on the basis of chemical order network model and the topological model. There is a minimum in the photocurrent observed at the 5 atomic percentage of indium concentration which is consistent with the minimum observed in the DC activation energy and the optical band gap of $\text{Se}_{90-x}\text{Sb}_{10}\text{In}_x$ ($0 \leq x \leq 15$) thin films [43].

4.1 Structure of bulk and thin films of $\text{Se}_{90-x}\text{Sb}_{10}\text{In}_x$ ($0 < x < 15$) system

The X-ray diffraction patterns of the $\text{Se}_{90-x}\text{Sb}_{10}\text{In}_x$ ($0 \leq x \leq 15$) bulk samples and thin films are shown in Fig. 4.1 and Fig 4.2, respectively. On the x-axis of the X-ray diffraction patterns the diffraction angle (2θ) varies from 10 - 60 degrees and on the Y-axis the intensity is represented in the arbitrary units. The absence of sharp peaks in the X-ray diffraction (XRD) pattern of $\text{Se}_{90-x}\text{Sb}_{10}\text{In}_x$ ($0 \leq x \leq 15$) (bulk and thin films) reveals the amorphous nature of the samples. It is observed from these figures that there -

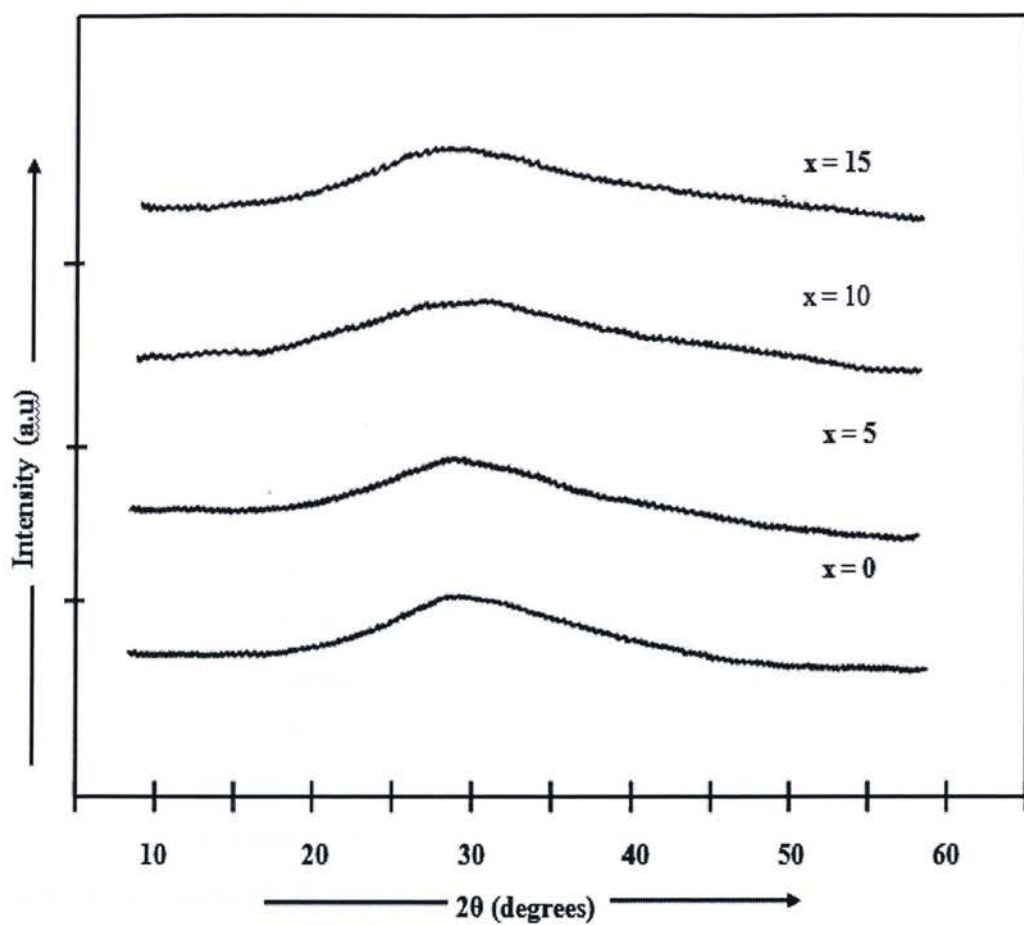


Figure 4.1 XRD pattern of bulk $\text{Se}_{90-x}\text{Sb}_{10}\text{In}_x$ ($0 \leq x \leq 15$)

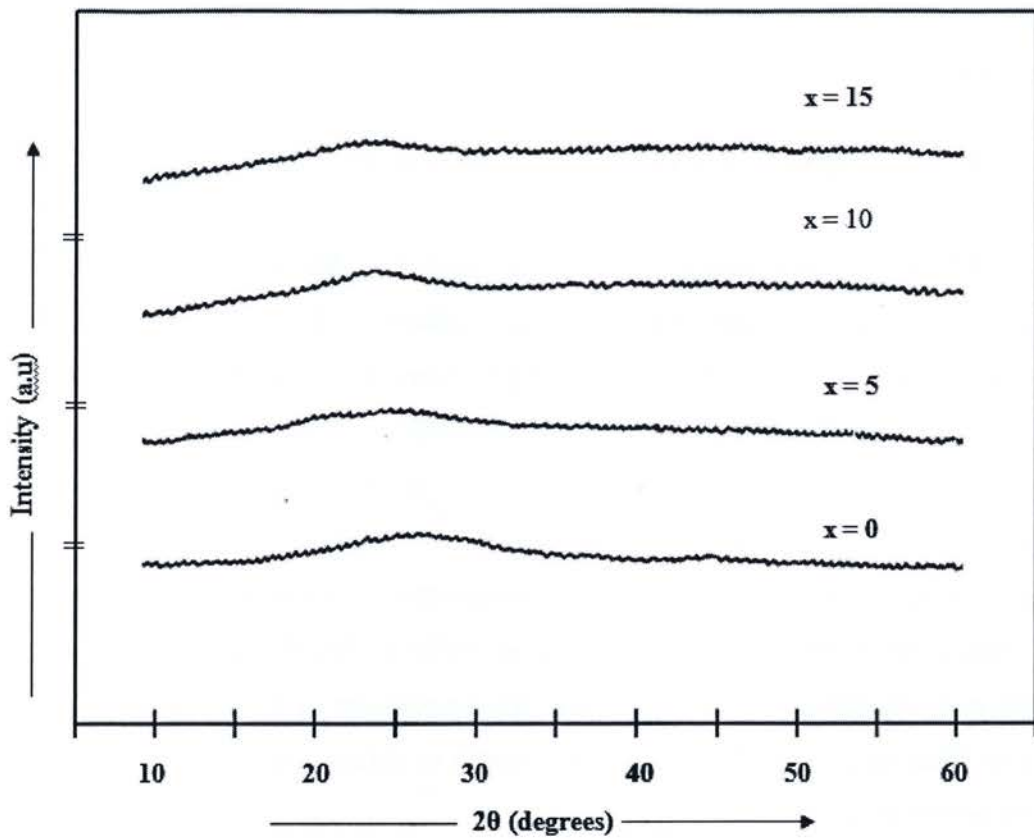


Figure 4.2 XRD pattern of $\text{Se}_{90-x}\text{Sb}_{10}\text{In}_x$ ($0 \leq x \leq 15$) thin films

-are broad humps in the XRD spectrum and the absence of sharp peaks in the spectrum, which indicates the amorphous nature of the bulk as well as thin films samples for $\text{Se}_{90-x}\text{Sb}_{10}\text{In}_x$ ($0 \leq x \leq 15$) system.

4.2 Composition analysis by ‘Rutherford back scattering technique

The composition analysis of thin films of all $\text{Se}_{90-x}\text{Sb}_{10}\text{In}_x$ ($0 \leq x \leq 15$) thin films was performed using Rutherford Back Scattering (RBS) technique as described in the section 3.4 of chapter 3. The results of RBS experiment are shown in Table 4.1. It can be seen from this table that final composition deposited on the thin films is very close to the starting composition. The RBS was carried out at different part of the same sample which confirmed the composition is uniformly distributed on each thin film sample. The percentage error between the starting composition and the obtained composition is also listed in the Table 4.1. It can be seen from Table 4.1 that the magnitude of the percentage error is negligible which indicate that the evaporation of the $\text{Se}_{90-x}\text{Sb}_{10}\text{In}_x$ ($0 \leq x \leq 15$) thin films by electron beam method is useful to obtain desired composition having up to three elements.

4.3 Photo-electrical properties of amorphous Se-Sb-In thin films

In this section a systematic study of photocurrent and photosensitivity of the electron beam evaporated thin films of amorphous $\text{Se}_{90-x}\text{Sb}_{10}\text{In}_x$ ($0 \leq x \leq 15$) has been carried out. The steady state photocurrent and transient photocurrent was measured. The effect of different illumination intensities (500 lux – 5000 lux) on the photoconduction has also been investigated. In addition, the effect of Indium addition to Se-Sb matrix on the photosensitivity has been studied.

The samples were characterized by using different techniques (XRD and RBS) as described in the chapter 3: Experimental Procedures and Design. The DC electrical conductivity of $\text{Se}_{90-x}\text{Sb}_{10}\text{In}_x$ ($0 \leq x \leq 15$) thin films was previously reported in [43] and it was found that the DC conductivity is activated in the entire temperature range from the temperature variation of DC conductivity. The DC activation energy of electrical -

Elements Sample	Se		Sb		In	
	Composition	% error	Composition	% error	Composition	% error
Se ₉₀ Sb ₁₀	89.980	-0.022	10.020	0.190	0.000	X
Se ₈₅ Sb ₁₀ In ₅	84.948	-0.061	10.023	0.220	5.032	0.640
Se ₈₀ Sb ₁₀ In ₁₀	80.011	0.0130	9.994	-0.060	9.995	-0.050
Se ₇₅ Sb ₁₀ In ₁₅	75.132	0.176	9.998	-0.090	14.870	-0.860

Table 4.1 Results of RBS and error percentage in composition

-conduction was determined from the slope of the temperature versus dc conductivity variation as reported earlier [43]. Since, in the present case there was a single slope observed from the plot of temperature versus DC conductivity, therefore the system Se-Sb-In exhibit only one type of conduction mechanism (activated type conduction) in the given temperature range.

4.4 Steady state photoconductivity

The variation of the photocurrent with light intensity is shown in Fig. 4.3. In this case, the light was illuminated on a thin film sample and the photocurrent was recorded after it became steady. The steady state photocurrent measurements were taken for different illumination intensities varying from 500 – 5000 lx. All the measurements were taken at the room temperature. It has been observed that this variation resulted in a straight line and obeys the power law given by the following equation:

$$I_{ph} \propto F^\gamma \quad (4.1)$$

where, I_{ph} is the photocurrent (total current minus dark current), F is the intensity of the light and γ is the exponent, which is calculated from the slope of the straight line resulted from the Intensity versus photocurrent variation. The exponent γ is a very important parameter, which determines the recombination mechanism in the semiconductor materials. The value of $\gamma = 0.5$ indicates a bimolecular recombination process, whereas $\gamma = 1.0$ indicates a monomolecular recombination mechanism. The recombination behaviour is difficult to understand in terms of discrete trap levels if the value of exponent γ lies between 0.5 and 1.0. It simply indicates the existence of continuous distribution of traps in the band gap [63].

In the present case the exponent γ lies between 0.5 and 1.0, which indicates there exists a continuous distribution of localized states in the mobility gap of a- $\text{Se}_{90-x}\text{Sb}_{10}\text{In}_x$ ($0 \leq x \leq 15$) thin films. Similar results for other chalcogenide thin film systems such as Se-Te-Pb were reported earlier [63].

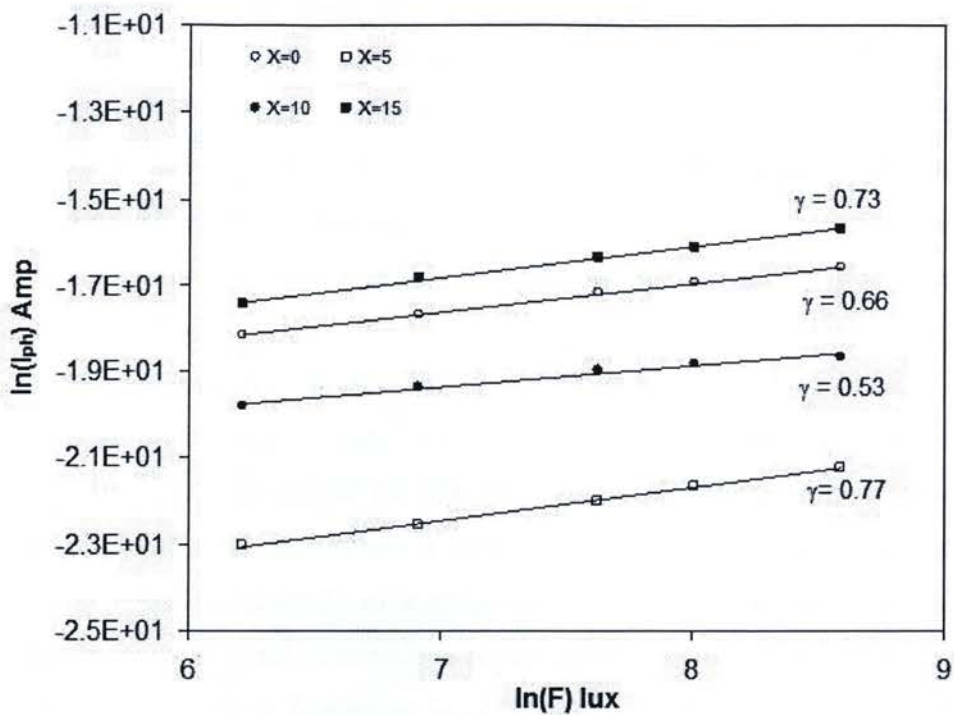


Figure 4.3 Variation of photo current I_{ph} with light intensity F for $Se_{90-x}Sb_{10}In_x$ ($0 \leq x \leq 15$)

4.5 Transient photoconductivity

The variation of the photocurrent in $\text{Se}_{90}\text{Sb}_{10}$ and $\text{Se}_{90-x}\text{Sb}_{10}\text{In}_x$ ($x = 15$) thin films with the exposure time at room temperature at different illumination intensities is shown in Figs. 4.4 & 4.5 respectively. All the other samples show a similar trend. It can be observed from these figures that the magnitude of the photocurrent is higher in the samples containing $\text{In} = 15$ at% as compared to the samples that do not have indium contents. It can also be seen from the figures 4.4 & 4.5 that when the samples are exposed to light, the photocurrent quickly reaches the maximum (5 -10 secs) and then it start decreasing with time and attains a nearly constant value in about 15 minutes.

These results are qualitatively consistent with the previous reported results [64-68]. It was reported that for As_2Se_3 samples, it took many hours for the photocurrent to attain a constant value at low light intensities and for higher light intensities; the photocurrent quickly attained the constant value [69]. It can also be seen from the figures 4.4 & 4.5 that photocurrent increase with the increase in illumination intensity of light (500 lx – 5000 lx). This type of behaviour can be explained in terms of charged defect model [1-2] and intercluster interaction model [65] as explained in the sections 4.8 and 4.9 of this chapter, respectively.

4.6 Compositional dependence of photocurrent of $\text{Se}_{90-x}\text{Sb}_{10}\text{In}_x$ ($0 < x < 15$) thin films

The composition dependence of photocurrent with exposure time at the illumination intensity of 5000 lx is shown in Fig. 4.6. It can be seen from this figure that photocurrent increases with the Indium concentration. However, the photocurrent shows a minimum at Indium concentration of 5 atomic percent. In Fig. 4.7 the y axis is restricted in-order to see the photocurrent variation with exposure time more clearly. Due to high magnitude of the photocurrent for Indium = 15 atomic percent, it is difficult to observe the variation of $\text{Se}_{90-x}\text{Sb}_{10}\text{In}_x$ ($0 \leq x \leq 15$) for ($x = 0, 5$ and 10) in Fig 4.6. It can be seen from figures 4.6

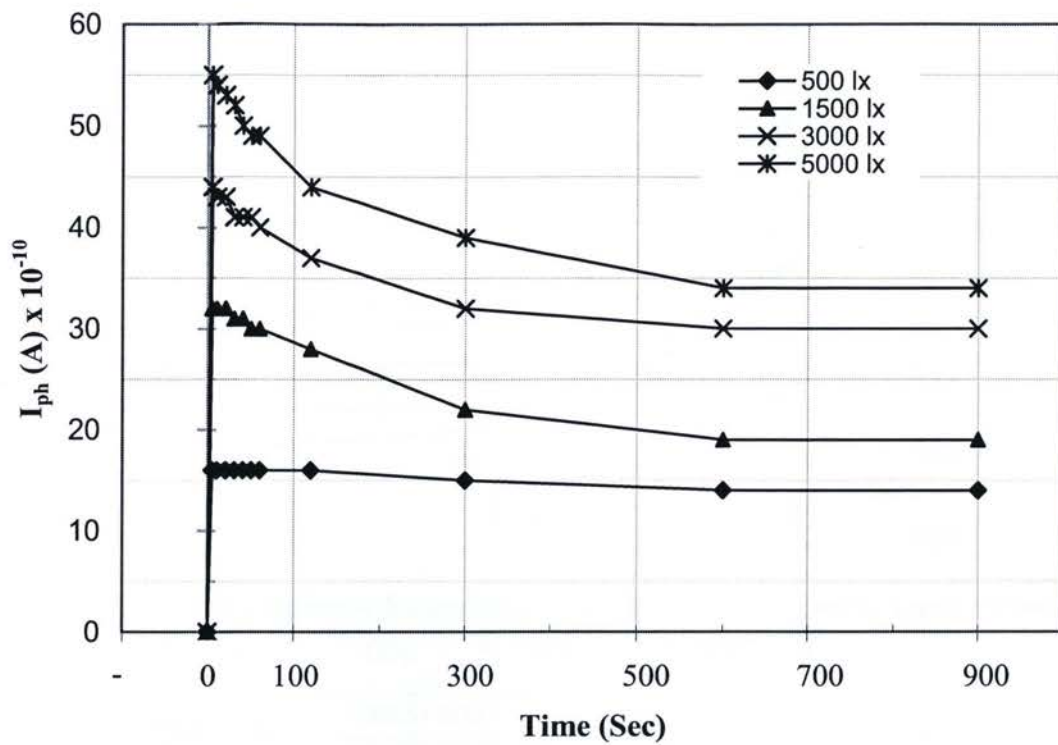


Figure 4.4 Transient photoconductivity of $Se_{90}Sb_{10}$

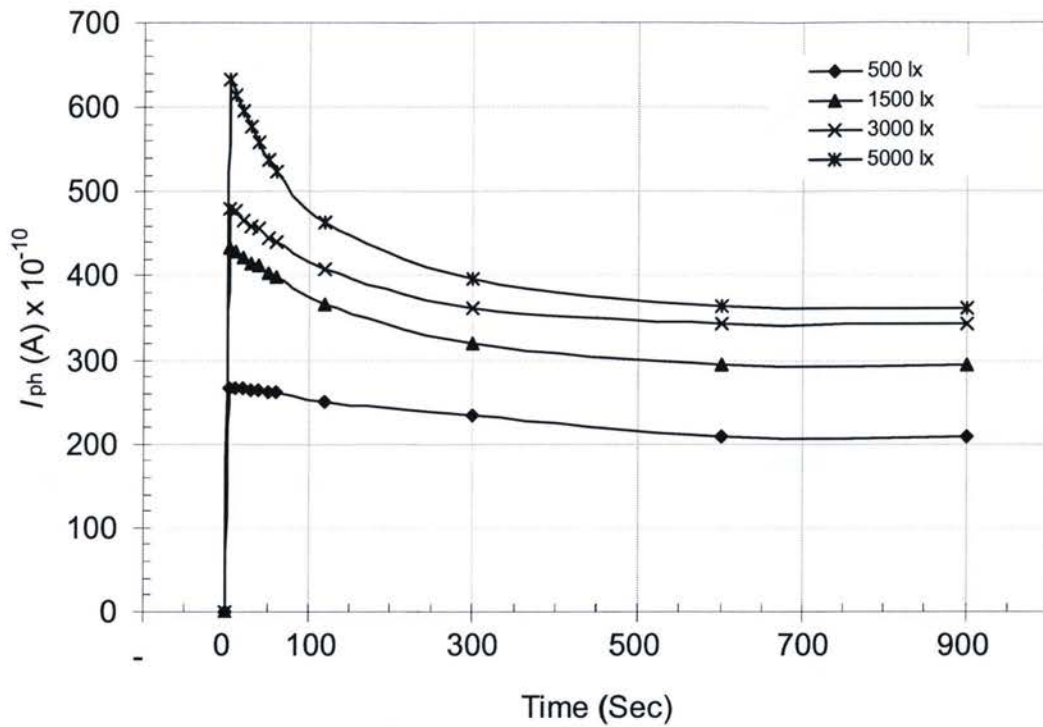


Figure 4.5 Transient photoconductivity of $\text{Se}_{90-x}\text{Sb}_{10}\text{In}_x$ ($x = 15$)

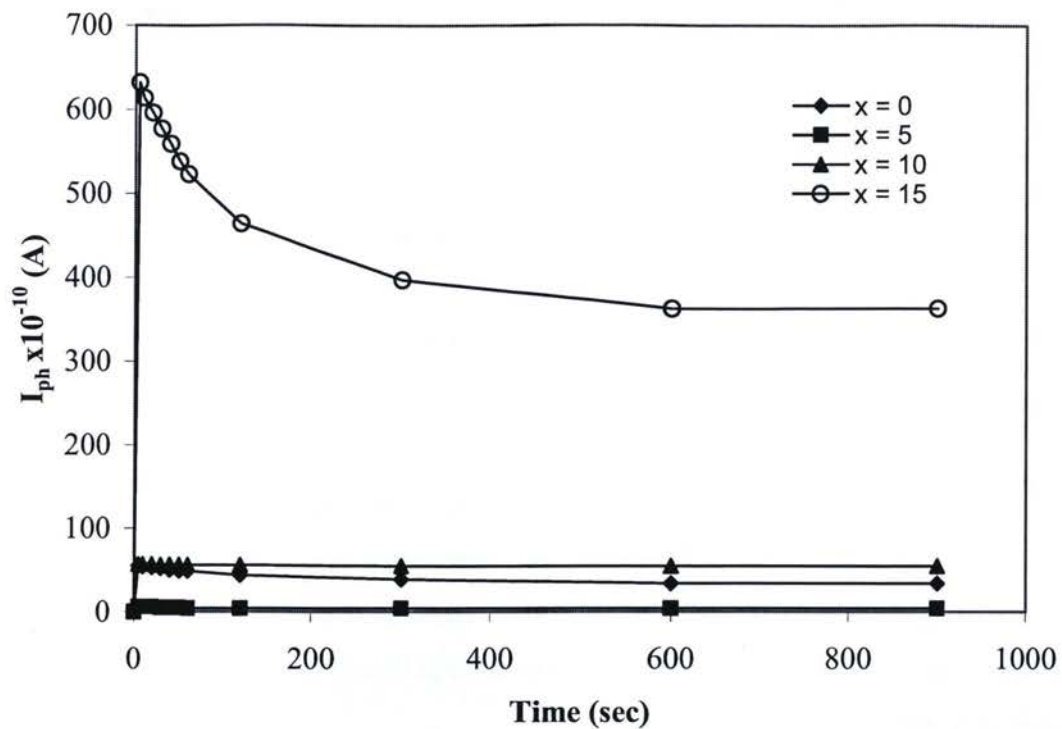


Figure 4.6 Compositional dependence of photocurrent versus exposure time at 5000 lx

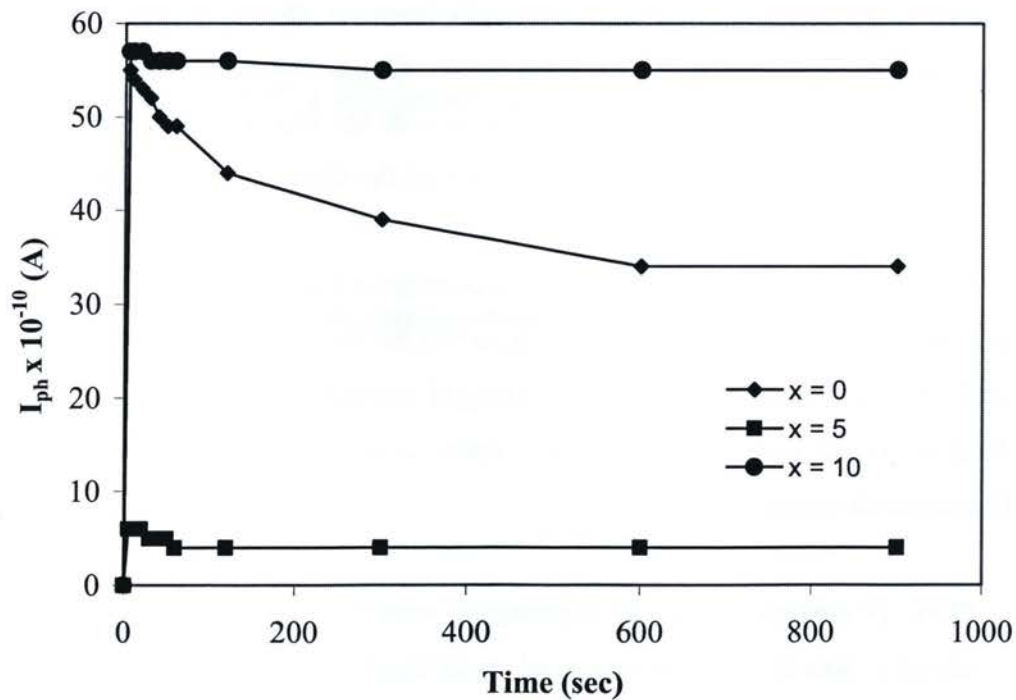


Figure 4.7 Compositional dependence of photocurrent versus exposure time at 5000 lx with restricted Y axis

and 4.7 that the photocurrent first reaches the maximum value then start decreasing and it becomes constant almost after 15 minutes of exposure.

4.7 Charged defect model

The photoconductive phenomenon in amorphous chalcogenide glasses can generally be understood in terms of the charged defect model [1] or the valence-alteration-pair model [70]. Considering these models for the amorphous chalcogenide glasses, the configuration coordinate diagram is shown in Fig. 4.8.

It can be seen from Fig. 4.8 that there exists three energy wells, indicating different defect energy states. The first energy well represents that the energy minimum of the photo-excited state is located above the D^0 (neutral dangling bond) state. The other energy wells are the defect state D^- and the normal bonding state NB of the chalcogenide system respectively.

The decrease in photocurrent with the exposure time at the room temperature can be related to the creation of D^- and D^+ centers, however, the existence of the D^+ centers is not essential here because in the present case the photocurrent in $\text{Se}_{90-x}\text{Sb}_{10}\text{In}_x$ ($0 \leq x \leq 15$) thin films at room temperature decreases with the illumination of light and D^+ comes into play only when photocurrent increases with the illumination of light.

As shown in Fig. 4.8 the D^- can be converted from D^0 centers with thermal energy at room temperature. It may be noted here that the thermal energy at room temperature is sufficient to create the negatively charged dangling bonds and positively charged dangling bonds also known as defect states as D^- and D^+ respectively of a particular chalcogenide system.

Now, D^- centres can act as trapping or recombination centers for holes due to the Coulomb's forces of attraction and accordingly the decrease in the photocurrent observed. These photo-induced charged defects are meta-stable and can be recovered to the normal bonding structures with annealing near the glass transition temperature.

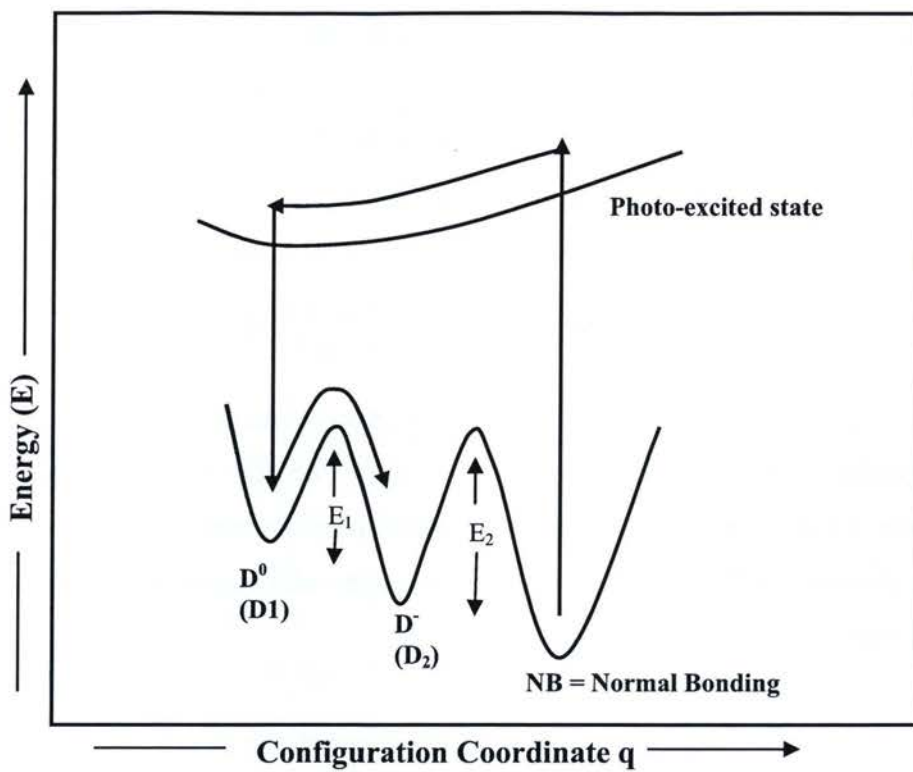


Figure 4.8 Configuration coordinate diagram

4.8 Inter-cluster interaction model

The decrease in the photocurrent during illumination of light can also be understood without the assumption of the bond breaking process upon illumination. The importance of the interaction between the lone-pair electrons of the chalcogenide atoms belonging to the different segmental and/or fragmental clusters has been explained by Ovshinsky [71].

It has been also reported that the lone pair electrons of the chalcogenide atoms interacting with each other through Van der Waals forces can induce the electrically neutral gap states. The quasi-stable states D^0 and D^- in the Fig. 4.8 can be replaced by the structures D_1 and D_2 respectively as shown in Fig. 4.8.

In chalcogenide glasses, the lone-pair electrons form the top of the valence band and the width of the valence band is governed by the interaction of these lone-pairs. As shown in Fig. 4.9a there exist a normal bonding site, where the interaction between lone-pair electrons of the chalcogen atoms is stronger, and consequently, the site can act as a hole trap.

Now, when the chalcogenide glass is illuminated, the electron-hole pair is excited, the hole can diffuse and electron is left behind which is less mobile. The hole may be captured by a hole trap which in turns trapped deeper through modifying the inter-cluster interactions i.e. the lattice relaxation takes place. At room temperature, thermal energy can excite the trapped electron, leaving the atomic structure unchanged.

The electron can diffuse and it can recombine with the trapped hole. In this case the atomic structure of a hole trap will partially be relaxed. As a result of which, the number of a hole trap increases (Fig. 4.9b), which is responsible of the decrease in the photocurrent with the exposure time during the illumination. The configuration diagram is applicable in the both of the above given models presented in the sections 4.8 & 4.9 respectively. The photodegradation which was observed in the $\text{Se}_{90-x}\text{Sb}_{10}\text{In}_x$ ($0 \leq x \leq 15$) thin films at room temperature can be reduced to material- dependence of the barrier height for energy well E_2 .

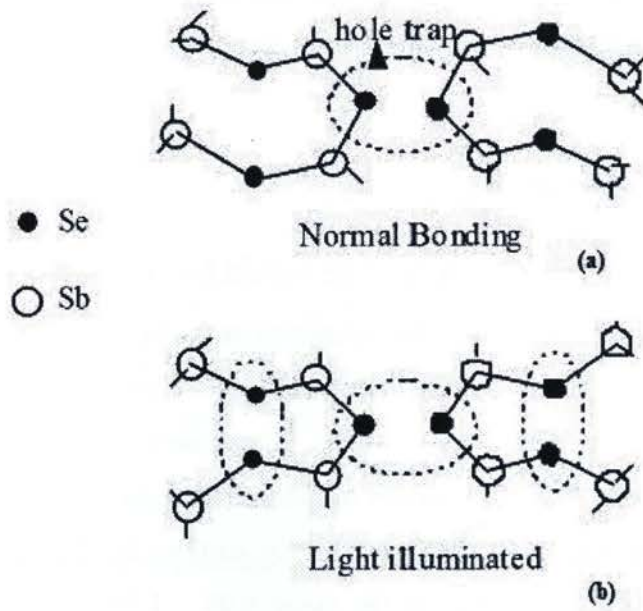


Figure 4.9 Schematic diagram of inter-cluster interaction model (a) Normal bonding (b) Structure influenced by light illumination

The quantity E_2 reflects the glass transition of the materials. If we can modify the glass transition temperature by adding some impurities, the parameter E_2 can be controlled and thereby reduce the photodegradation. The energy barrier E_1 exists at the low temperature due to defect states. The value of energy barriers E_1 and E_2 can be calculated from the measured lifetimes of the photo-degraded states through assuming the thermally activated relaxation [65]. i.e.

$$\frac{1}{\tau(T)} = \Omega \exp \left[-\frac{E_b}{k_B T} \right] \quad (4.2)$$

E_b (= barrier height) = E_1 or E_2 , $\tau(T)$ is the typical lifetime of the photo-degraded state as a function of temperature and can be calculated as the procedure given elsewhere [63], Ω is the vibrational frequency and in the present case is taken to be $\Omega = 10^{13}$ Hz and k_B is Boltzmann constant. The values of E_2 is calculated using the glass transition temperature in equation (4.2), The values of glass transitions temperature of $\text{Se}_{90-x}\text{Sb}_{10}\text{In}_x$ ($0 \leq x \leq 15$) lies between 322-328K as reported earlier [21]. Using equation (4.2), the value of E_1 and E_2 are found to be in the range 0.99 – 1.05 eV and, 1.068 – 1.123 eV respectively, for different light intensities (500 lx to 5000 lx) for $\text{Se}_{90}\text{Sb}_{10}$ thin films. In case of Indium doped samples, the value of E_1 and E_2 lies between 1.01 – 1.04 eV and 1.11 – 1.139 eV respectively, for different light intensities (500 lx to 5000 lx). The above values of E_1 and E_2 are in close agreement with the values reported for other chalcogenide systems such as a- As_2S_3 , a- As_2Se_3 and a- As_2Te_3 [65].

4.9 Influence of bias voltage on dark current and photocurrent of $\text{Se}_{90-x}\text{Sb}_{10}\text{In}_x$ ($0 < x < 15$) thin films

The current-voltage (I - V_B) characteristics of $\text{Se}_{90}\text{Sb}_{10}$ and $\text{Se}_{75}\text{Sb}_{10}\text{In}_{15}$ thin films samples at different bias voltages for dark current and current resulted for light illumination are shown in Figures 4.10 and 4.11, respectively. All the other samples show a similar trend. The straight lines passing through the origin confirm the Ohmic nature of the electrical contacts for the present samples. Differential conductance $\left(\frac{dI}{dV} \right)$ is calculated from the slope of (I - V_B) plots.

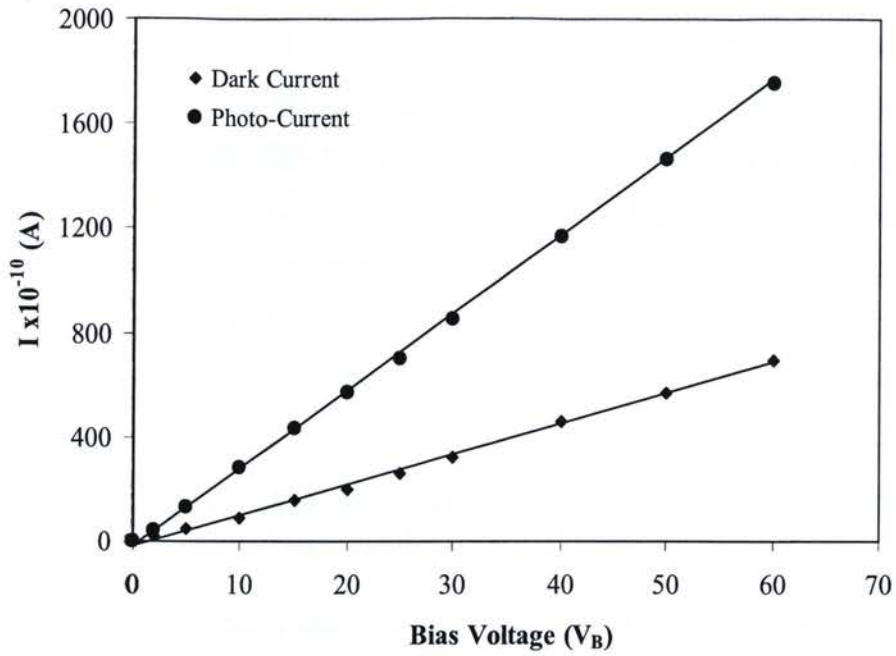


Figure 4.10 Variation of bias voltage with current of $\text{Se}_{90}\text{Sb}_{10}$

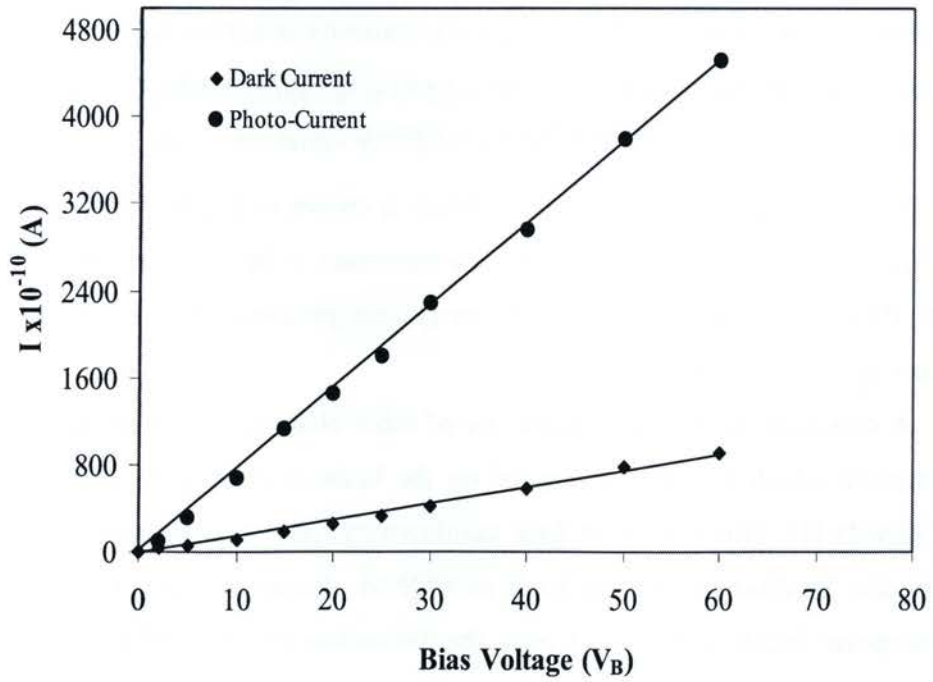


Figure 4.11 Variation of bias voltage with current of $\text{Se}_{75}\text{Sb}_{10}\text{In}_{15}$

The value of differential conductance for all the thin film samples calculated at room temperature and at 1000 lx is listed in Table 4.2. It can be seen from this table that the value of differential conductance is higher in case of illuminated samples than the samples studied under dark. The higher value of differential conductance in case of light illuminated samples is expected due to the decrease in resistivity of thin film samples upon illumination. Similar results were reported for the Sb_2Se_3 chalcogenide system [65]. The value of differential conductance is found to be minimum for the samples having Indium content equal to 5 % as seen from Table 4.2.

4.10 Compositional dependence of dark conductivity, photoconductivity and photosensitivity

The composition dependence of the dark and photoconductivity measured at room temperature is shown in Fig. 4.12. It can clearly be seen from this figure that both dark conductivity and photoconductivity shows a minimum at 5 at.% of Indium composition. Both the dark conductivity and the photoconductivity initially decreases with addition of Indium up-to 5at.%, thereafter, these parameters start increasing with increase in Indium concentration (up-to 15 at.%). The photosensitivity is accounted for the use of particular material in the photoconductive devices and it is calculated by dividing the photo current by dark current (I_{ph} / I_d). The photosensitivity variation of the $\text{Se}_{90-x}\text{Sb}_{10}\text{In}_x$ ($0 \leq x \leq 15$) with composition and at room temperature is shown in Fig 4.13. It can be seen from this figure that photosensitivity also show a minimum at $\text{In} = 5$ at%, The similar variation in the dark conductivity, photoconductivity and photosensitivity was observed in other chalcogenide systems.

A minimum in the photosensitivity of other chalcogenide systems at $\text{In} = 4$ at.% was observed which has been discussed on the basis of chemically ordered network model (CONM) [1]. Our results of dark conductivity, photoconductivity and photosensitivity can also be discussed on the basis of CONM. According the CONM, the formation of hetropolar bonds is favoured over the formation of homopolar bonds and the glassy structure is assumed to be composed of cross-linked--structural units of the stable chemical compounds (hetropolar bonds) of the system and excess, if any, of the elements

Sample	Differential Conductance (Dark) nS	Differential Conductance (Illumination) nS
x = 0	1.20	3.00
x = 5	0.02	0.80
x = 10	1.50	7.72
x = 15	4.71	5.71

Table 4.2 Differential conductance of $\text{Se}_{90-x}\text{Sb}_{10}\text{In}_x$ ($0 \leq x \leq 15$) thin films at room temperature at 1000 lx

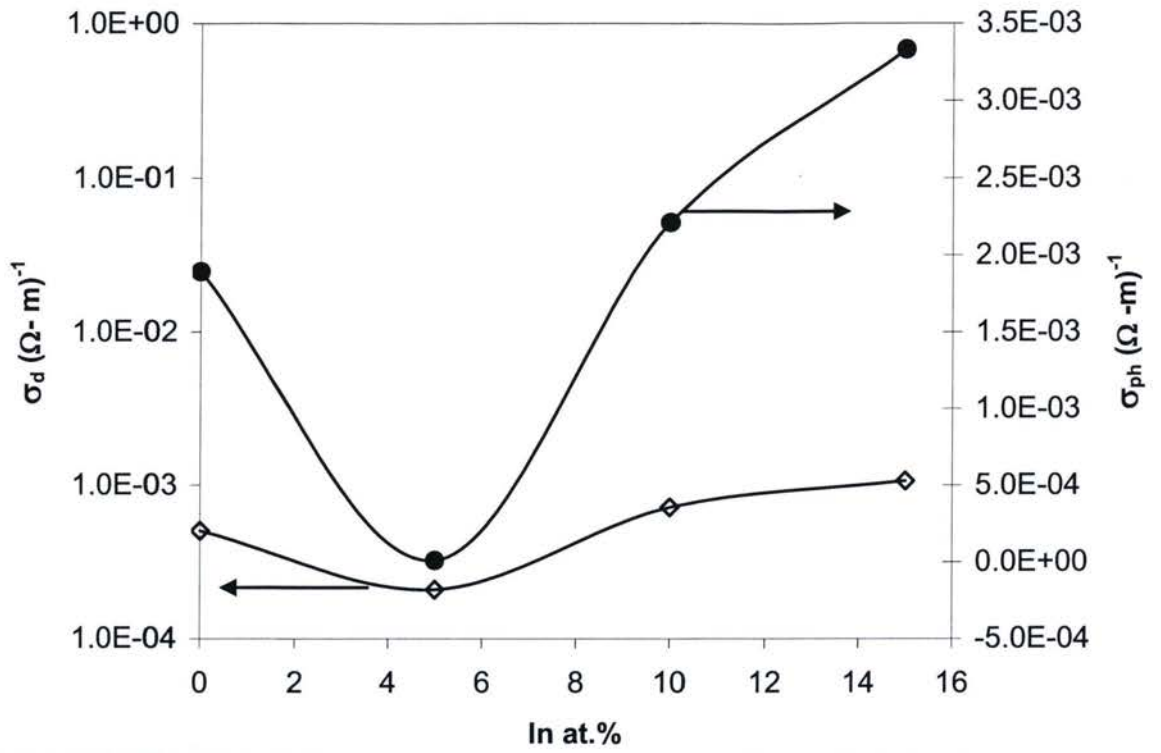


Figure 4.12 Variation of dark conductivity (σ_d) and photoconductivity (σ_{ph}) with composition

(homopolar bonds). Due to chemical ordering features, such as, change in slope or a kink occur for the various properties and parameters at the stoichiometric compositions at which the glass structure is made up of cross-linked structural units consisting of heteropolar bonds only. The tie line compositions, where the features have chemical origin, are also referred to as the chemical threshold of the system [72-73].

The compositional dependence of the photosensitivity can also be explained in terms of Topological models and the average coordination number $\langle z \rangle$ of Se-Sb-In. The average coordination number $\langle z \rangle$ in the present case is calculated by using the standard method [75] defined by:

$$\langle z \rangle = 8 - \left[\frac{6a + 5b + 3c}{100} \right] \quad (4.3)$$

where 6, 5 and 3 are the valence electrons for Se, Sb and In respectively, and a, b and c are their respective concentrations in the glass composition. It was reported that at $\langle z \rangle = 2.4$, the glass network changes from an elastically floppy (polymeric glasses) type to a rigid type (amorphous solid) [70].

The topological model when extended to medium range structures for other chalcogenide systems, a discontinuity in the physical parameters at $\langle z \rangle = 2.67$ was reported in the literature [70], according to which, the features present at $\langle z \rangle = 2.67$ were attributed to a change from two dimensional layered type structure to three dimensional network arrangement due to cross linking. In the present case a discontinuity at an average coordination number of $\langle z \rangle = 2.25$, which is similar to the topological models based on the constraints theory described above.

A minimum in optical band gap and the activation energy at $\langle z \rangle = 2.25$ (In = 5 atomic percentage) (also shown in Fig. 4.13) was already reported elsewhere [43] and also the minimum in the peak crystallization temperature at In = 5 atomic percentage suggests some kind of structural changes taking place in the Se-Sb-In system [21].

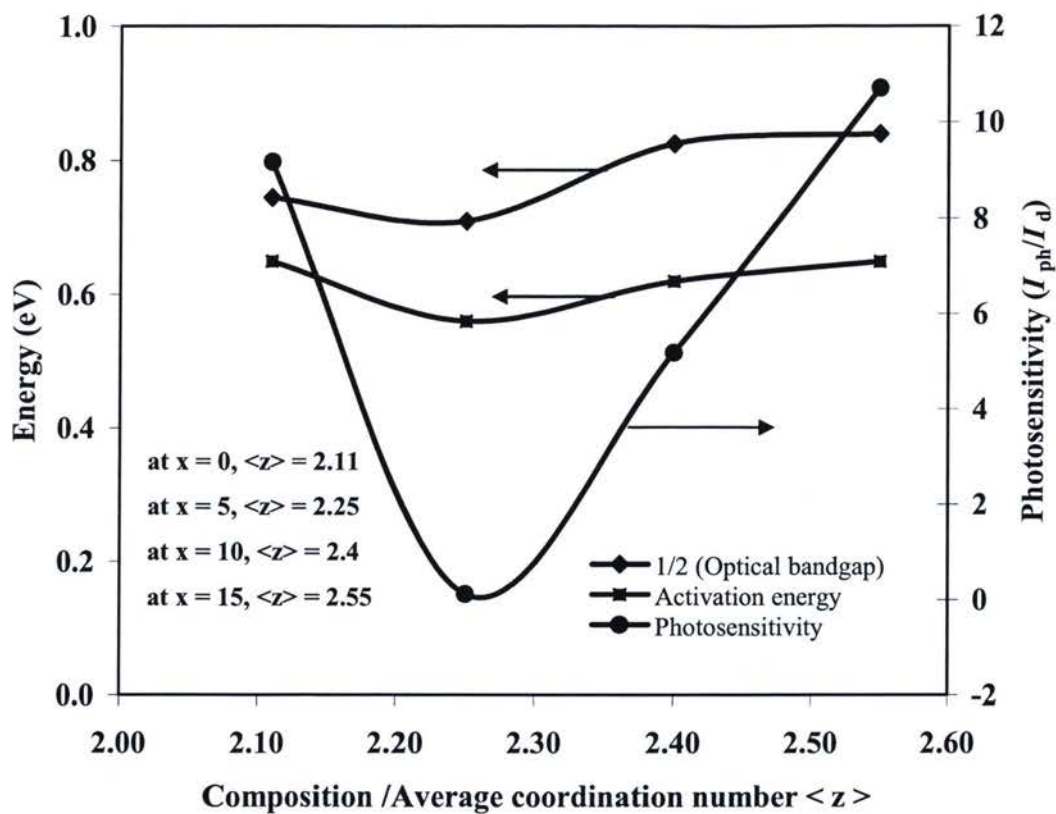


Figure 4.13 Composition/Average coordination dependence of photosensitivity of $\text{Se}_{90-x}\text{Sb}_{10}\text{In}_x$ ($0 \leq x \leq 15$) thin films

Chapter 5

5 Summary and Conclusions

This chapter includes the summary and conclusions drawn from the present study. The scope of the future work has also been presented in this chapter.

- Bulk samples of $\text{Se}_{90-x}\text{Sb}_{10}\text{In}_x$ ($0 \leq x \leq 15$) system were prepared by conventional melt quenching technique and the thin films were prepared by electron beam evaporation. Following conclusions are drawn from the present study.
- The samples (bulk as well as thin films) were amorphous in nature as revealed from the absence of sharp peaks in X-ray diffraction spectrum.
- The steady state and transient photoconductivity measurements have been carried out in the $\text{Se}_{90-x}\text{Sb}_{10}\text{In}_x$ ($0 \leq x \leq 15$) thin films. From the steady state measurement it has been found that there exist continuous distributions of localized states in the mobility gap of $\text{Se}_{90-x}\text{Sb}_{10}\text{In}_x$ ($0 \leq x \leq 15$) chalcogenide system.
- The phenomenon so-called photodegradation in the photocurrent has been observed with the illumination during the transient photoconductivity measurements of $\text{Se}_{90-x}\text{Sb}_{10}\text{In}_x$ ($0 \leq x \leq 15$) thin films, i.e., the photocurrent decreases upon illumination with exposure time. The photocurrent attains nearly a constant value after approximately 15 minutes of exposure to light.
- The transient photoconductivity measure indicates that the magnitude photocurrent is maximum for the samples containing highest value of Indium concentration (In = 15 atomic percentage). The minimum photocurrent is observed for the samples having 5 atomic percentage of Indium in Se-Sb-In thin

films. From the above observation, it is recommended to use $\text{Se}_{75}\text{Sb}_{10}\text{In}_{15}$ particular composition for the application in the photoconductors devices because of its high magnitude of photocurrent.

- Different models have been used to explain the decrease in photocurrent upon light illumination. The potential energy barrier heights (E_1 and E_2) are calculated using the differential life-time (τ) and the glass transition temperature.
- The dark current and the photocurrent increase with increasing bias voltage. The differential conductance calculated from the slope of current versus voltage plots, show a minimum at 5 atomic percentage of indium concentration.
- Dark conductivity, photoconductivity and photosensitivity studies show a minimum at 5 atomic percentage of Indium concentration. Chemically Ordered Network (CONM) model and Topological model were used to explain the minimum in the photosensitivity. The decrease in the photosensitivity at $\text{In} = 5\text{at.}\%$ is also consistent with the previous results [43] which show a minimum in the optical band gap and DC activation energy, therefore, indicating the changes in the structure and network of $\text{Se}_{90-x}\text{Sb}_{10}\text{In}_x$ ($0 \leq x \leq 15$) semiconducting system at $\text{In} = 5$ atomic percentage concentration.

5.1 Scope of future work

Although a great deal of information has been gathered from the present investigations, additional studies must be undertaken in order to have a better knowledge of the chalcogenide systems. Some of the studies, which can be carried out, are given below:

- The role of substrate temperature in light-induced changes in optical and electrical properties of thin films of sample should be investigated. The photo-darkening studies should be carried in order to investigate the photodegradation in the photocurrent.
- Raman spectroscopy and Fourier transform infrared (FTIR) Spectroscopy studies should be employed in order to have knowledge about the irradiation induced structural changes in the thin films of all samples.

- We also intended to use the $\text{Se}_{75}\text{Sb}_{10}\text{In}_{15}$ material (cost effective) in the thermal imaging applications. Normally the expensive Ge-alloy lens is being used in the thermal imaging cameras. We plan to fabricate the $\text{Se}_{75}\text{Sb}_{10}\text{In}_{15}$ lens to be replaced with the Ge-alloy lens and to compare and analyze the results. The research on using the chalcogenide-based lens in thermal imaging cameras is still ongoing and there are many challenges to be addressed in-order to attain the desired results of thermal imaging [75].
- Photoluminescence studies should also be performed on the irradiated and un-irradiated samples.
- The a.c. conductivity of all the samples should be performed to have an idea about the defects present in the system both for illuminated and virgin chalcogenide systems.

6 References

- [1] S.R. Elliott, "Physics of amorphous materials", Longman Scientific & Technical and John Wiley & Sons, New York, 1990.
- [2] S.R. Elliott, "A unified model for reversible photostructural effects in chalcogenide glasses," *Journal of Non-Crystalline Solids*, 81 (1986) 71.
- [3] C.A. Angell, "Perspective on the glass transition", *Journal of Physics and Chemistry of Solids*, 49 (1988) 863.
- [4] K. Morigaki, "Physics of amorphous semiconductors", Imperial College Press, London, (1999).
- [5] F. Jedema, Phase-change materials: Designing optical media of the future, *Nature Materials*, 6 (2007) 90.
- [6] D.J. Milliron, S. Raoux, R.M. Shelby and J.J. Sweet, "Solution-phase deposition and nano-patterning of GeSbSe phase- change materials", *Nature Materials*, 6 (2007) 352.
- [7] K. Rosan, "Amorphous and microcrystalline semiconductors devices", Eds. J. Kanicki, pp 281, 1991.
- [8] S.R. Ovshinsky, "Insulating and semiconducting glasses", Eds. P. Boolchand, World Scientific Press, Singapore, pp737, 2000.
- [9] B. Liu, Z Song, S. Feng and B. Chen, Characteristics of chalcogenide nonvolatile memory nano-cell-element based on Sb₂Te₃ material," *Microelectronic Engineering* 82 (2005) 168.
- [10] "Chalcogenide memory Industry", III Vs Review, 18 (2005) 15. doi:10.1016/S0961-1290(05)71331-4
- [11] K.V. Reddy, A.K. Bhatnagar, "Electrical and optical studies on amorphous Se-Te alloys", *Journal of Physics D: Applied Physics*, 25 (1992) 1810.
- [12] H. B. Chung, K. Shin, and J. M. Lee, "Phase-change characteristics of chalcogenide Ge₁Se₁Te₂ thin films for use in nonvolatile memories", 25 (2007) 48.

- [13] P.R. de Moura, D.P. Almeida and J.C. de Lima, "Electro-photographic photoreceptors including selenium-based multilayers", *Journal of Electron Spectroscopy and Related Phenomena*, 155 (2007) 129.
- [14] K. Tanaka, A. Odajima, "Photodarkening in amorphous Selenium", *Solid State Communications*, 43 (1982) 961.
- [15] M. Frumar, B. Frumarova, P. Nemeč, T. Wagner, J.J. Jedelsky and M. Hrdlicka, "Thin chalcogenide films prepared by pulsed laser deposition - : new amorphous materials applicable in optoelectronics and chemical sensors" 352 (2006) 544.
- [16] H.Y. Zhang, Z.Q. Hu, K. Lu, "Transformation from the amorphous to the nanocrystalline state in pure selenium", *Nanostructured Materials*, 5 (1995) 41.
- [17] T. Fukunaga, M. Utsumi, H. Akatsuka, M. Misawa, U. Mizutani, "Structure of amorphous Se prepared by milling", *Journal of Non-Crystalline Solids*, 205-207 (1996) 531.
- [18] G.J. Fan, F.Q. Guo, Z.Q. Hu, M.X. Quan and K. Lu, "Amorphization of selenium induced by high-energy ball milling", *Physical Review B*, 55 (1997) 11010.
- [19] J.C Lima, T.A. Grandi, R.S. de Biasi, "Influence of aging on the thermal and structural properties of amorphous selenium prepared by ball milling", *Journal of Non-Crystalline Solids*, 286 (2001) 93.
- [20] J.C. Lima, V.H.F. Das Santos and T.A. Grandi, "Structural study of the Zn-Se system by ball milling technique", *Nanostructured Materials*, 11 (1999) 51.
- [21] G. Kaur and T. Komatsu, "Crystallization behavior of bulk amorphous Se-Sb-In System", *J. Mater Sci.* 36 (2001) 4531.
- [22] Y.M. Yiu, T.K. Sham and G Kaur, "Electronic structure of Se, Se-Te, and Se-Te-Sb systems: Some observations from the x-ray spectroscopy and *ab initio* calculations", *Journal of Applied Physics*, 104 (2008) 013713.
- [23] A.S. Soltan, A.A. Abu. Sehly and M.A. Abdel-Rahim, "Effect of composition and thermal annealing on the absorption and electrical conduction of $\text{Se}_{85-x}\text{Te}_{15}\text{Sb}_x$ glasses", *Journal of Physics and Chemistry of Solids*, 63 (2002) 801.
- [24] A.S. Soltan, "Calorimetric study of the chalcogenide glass $\text{Se}_{77}\text{Te}_{20}\text{Sb}_3$ ", *Physica B*, 307 (2001) 78.

- [25] V Sharma, A. Thakur, N Goyal, G.S.S. Saini and S.K. Tripathi "Effect of In additive on the electrical properties of Se-Te alloy", *Semiconductor Science and Technology*, 20 (2005) 103.
- [26] G. Kaur, T. Komatsu and R. Thangaraj, "Crystallization kinetics of bulk amorphous Se-Te-Sn system", 35 (2000) 903.
- [27] W. Zhiya, T. Changjian, Li. Yanamei and C. Quanjiang, "The effects of Sn and Bi additions on properties and structure in Ge-Se-Te chalcogenide glass", *Journal of Non-Crystalline Solids*, 191(1995) 132.
- [28] O.EI-Shazly, T. Ramandam, N. El. Anamy, H.A. Mataweh and E.F. EI-Wahidy, "Calorimetric studies of chalcogenide glasses in the system Se-S", *European. Physical. Journal-Applied Physics* 13 (2001) 161.
- [29] N.B. Maharajan, K. Singh, N.S. Sexena, "Calorimetric studies in $Se_{75}Te_{25-x}Sn_x$ chalcogenide glasses ", *Physica Status Solidi (a)*, 195 (2003) 305.
- [30] R.M. Mehra, A. Ganjoo, G. Kaur, P.C. Mathur, "Effect of in impurity on crystallization kinetics of $(Se_{.7}Te_{.3})_{100-x}In_x$ system", *Journal of Thermal Analysis and Calorimetry*, 45 (1995) 405.
- [31] A.S. Maan, D. R. Goyal , A. Kumar, "Investigation of optical absorption in $Te_5(In_xSe_{100-x})_{95}$ glassy alloys", *Chalcogenide Letters*, 4 (2007) 48.
- [32] V. Sharma, "Effect of Sn additive on the electrical properties of Se-Te glassy alloy", *Journal of Optoelectronics and Advanced Materials*, 8 (2006) 1823.
- [33] K. Balcerek, R. Nawryk, Cz. Marucha, K. Purczewski and Z.G. Ivanova, "Electrical resistivity and thermoelectric power of polycrystalline and amorphous Se-Te-Cu system", *Cryogenics*, 38 (1998) 1233.
- [34] K. Tanaka, N. Kawakami, A. Odajima, "Photoinduced elastic changes in amorphous As_2S_3 films", *Japanese. Journal of Applied Physics* 20 (1981) 874.
- [35] J. Teteris and M. Reinfelde, "Application of amorphous chalcogenide semiconductor thin films in optical recording technologies", *Journal of Optoelectronics and Advanced Materials*, 5 (2003) 1355.
- [36] K.E. Asatryan, S. Frederick, T. Galstian and R. Vallee, "Recording of polarization holograms in photodarkened amorphous chalcogenide films", *Applied Physics Letters*, 84 (2004) 1626.

- [37] A. Zakery and S.R Elliott, Springer Series in Optical Sciences," Optical Nonlinearities in Chalcogenide Glasses and Their Applications", Springer, Vol. 135 (2007).
- [38] A.V. Kolobov and J. Tominaga, Journal of Materials Science: Materials in Electronics, "Chalcogenide glasses as prospective materials for optical memories and optical data storage", 14 (2003) 677.
- [39] K.L. Bhatia, P. Singh, N. Kishore, S.K. Malik, "Electronic conduction in MeV energy ion-beam irradiated semiconducting glass $Pb_{20}Ge_{19}Se_{61}$ ", Philosophical Magazine B, 72 (1995) 417.
- [40] T. Tesvetkova, E. Amove, E. Vateva, V. Averyanov, "Ion Implantation Induced Modification of Vitreous Chalcogenides", Physica Status Solidi (a), 119 (1990) 107
- [41] P. Singh, K.L. Bhatia, N. Kishore, M. Singh, S.K. Malik, D. Kanjilal, "Doping of chalcogenide glassy semiconductor by implanting Ni ions", Journal of Non-Crystalline Solids, 191 (1995) 146.
- [42] J. Singh and K Tanaka, "Photo-structural changes in chalcogenide glasses during illumination", 18 (2007) 480.
- [43] M.S. Kamboj, G. Kaur, R. Thangaraj and D.K. Avasthi, "Effect of heavy ion irradiation on the electrical and optical properties of amorphous chalcogenide thin films", J. Phys. D: Appl. Phys. 35 (2002) 477.
- [44] M. Singh, "Effect of impurity addition and irradiation on some physical properties of Se-based chalcogenide semiconductors", Ph.D Thesis, 2004
- [45] M. Kastner, "Bonding bands, lone-pair bands, and impurity states in chalcogenide semiconductors", Physical Review Letters 28 (1972) 355.
- [46] S.R. Ovshinsky, K. Sapru, "Amorphous and liquid semiconductors", Eds. J. Stuke, W. Brenig, 1974.
- [47] R. Atta-Fynn, P. Biswas, P. Ordejo'n, and D. A. Drabold, "Systematic study of electron localization in an amorphous semiconductor", Physical Review B 69 (2004) 085207.
- [48] M.H. Cohen, H. Fritzsche and S.R. Ovshinsky, "Simple band model for amorphous semiconducting alloys", Physical Review Letters, 22 (1969) 1065.
- [49] N.F. Mott, E.A. Davis, Electronic processes in non-crystalline materials, Oxford, 1979.

- [50] E.A. Davis, N.F. Mott, "Conduction in non-crystalline systems V. Conductivity, optical absorption and photoconductivity in amorphous semiconductors", *Philosophical Magazine*, 22 (1970) 903.
- [51] J.M. Marshal, A.E. Owen, "Drift mobility studies in vitreous arsenic triselenide", *Philosophical Magazine*, 24 (1971) 1281.
- [52] A.E. Owen, W.E. Spear, "Electronic properties and localized states in amorphous semiconductors", *Physics and Chemistry of Glasses*, 27 (1976) 174.
- [53] R.A. Street, N.F. Mott, "States in the gap in glassy semiconductors", *Physical Review Letters*, 35 (1975) 1293.
- [54] N.F. Mott, E.A. Davis and R.A. Street, "States in the gap and recombination in amorphous semiconductors", *Philosophical Magazine*, 32 (1975) 961.
- [55] N.F. Mott and R.A. Street, "States in the gap in chalcogenide glasses", *Philosophical Magazine*, 36 (1977) 33.
- [56] M. Kastner and H. Fritzsche, "Defect chemistry of lone-pair semiconductors", *Philosophical Magazine*, 37 (1978) 199.
- [57] D. Alder, "Defects in amorphous semiconductors", *Journal of Non-Crystalline Solids*, 35 & 36 (1980) 819.
- [58] N.F. Mott, "Electrons in disordered structures", *Advances in Physics* 16 (1967) 49.
- [59] S.R. Ovshinsky, Proc. 7th Int. Conf. On Amorphous and Liquid Semiconductors, Edinburg 1977.
- [60] H. Mahr, "Absorption band shape and Urbach's rule of localized excitons", *Physical Review* 132 (1963) 1880.
- [61] J. Tauc, *Amorphous and Liquid Semiconductors*, Plenum, New York (1974) 569.
- [62] S. Tolonsky, "An introduction to interferometry, 2nd Ed. (Longman, London) 1973, pp214.
- [63] M.S. Kamboj, G. Kaur and R. Thangaraj, "Dark and Photoconductivity of amorphous Se-Te-Pb thin films", *Thin Solid Films*, 420-421(2002) 350.

- [64] P. Kumar and R. Thangaraj, Analysis of bias field influenced recombination processes in narrow gap Sb_2Se_3 thin films, *Journal of Condensed Matter Physics*, 20 (2008) 095213.
- [65] N. Toyosawa and K. Tanaka, "Photocurrent enhancement in light-soaked chalcogenide glasses", *Physical. Review B*, 56 (1997) 7416.
- [66] K. Shimakawa, S. Inami, T. Kato and S.R. Elliott, "Origin of photoinduced metastable defects in amorphous chalcogenides", *Physical. Review B*, 46 (1992) 10062.
- [67] N. Manikandan, B.H. Sharmila and S. Asokan, "Photoconductivity studies on bulk As-Te-In glasses", *Applied Physics A*, 81(2005) 1313.
- [68] P. Bhardwaj, P.K. Shishodia and R.M. Mehra, "Photoinduced degradation in the electrical properties of normally and obliquely deposited As_2Se_3 thin films", *Materials Science-Poland*, 25 (2007) 69.
- [69] P. Kounavis, E. Mytilineou, "The kinetics of the reversible light-induced phenomenon of sputtered amorphous As_2Se_3 ", *Philosophical Magazine Letters*, 72 (1995) 117.
- [70] S. Singh, R.S. Sharma, R.K. Shukla and A. Kumar "Steady state photoconductivity in a- $\text{Se}_{90}\text{Ge}_{10-x}\text{In}_x$ thin films", *Chalcogenide Letters*, 1 (2004) 83.
- [71] S.R. Ovshinsky and D. Adler, "Local structure, bonding, and electronic properties of covalent amorphous semiconductors", *Contemporary Physics*, 19 (1978) 109.
- [72] K. Tanaka, "Structural phase transitions in chalcogenide glasses", *Physical. Review B*, 39 (1989) 1270.
- [73] P. Boolchand, *Proceedings of International conference on Key Engineering Materials (Banglore-India) 13-15 (1987) 131.*
- [74] G. Saffarini and A. Schlieper, *Applied Physics A*, 61 (1995) 29.
- [75] X. Jhang, H. Ma and J. Lucas, Applications of chalcogenide glass bulks and fibres, *J. Optoelectronics and Advanced Materials*, 5 (2003) 1327.

7 List of publications

- M. Kamboj and F Mohammadi, "Steady state and transient photoconductivity measurements in a- $\text{Se}_{90-x}\text{Sb}_{10}\text{In}_x$ thin films", Submitted for publication at the IEEE Journal of Electronic Materials, November 2008.
- M. Kamboj and F. Mohammadi, "Photoconductivity measurements in amorphous $\text{Se}_{90-x}\text{Sb}_{10}\text{In}_x$ thin films" Accepted for presentation at the International Conference on Metallurgical Coatings and Thin Films (ICMCTF 2009), San Diego, USA, April 27-May 1, 2009.

3/6/09